A multi-scale approach for numerical modelling of the CO_2 sequestration process

A thesis submitted to the Section of Petroleum Engineering, Delft University of Technology, The Netherlands, for the degree of Master of Science.

By

Duaa Alshiroofi

In partial fulfilment of the requirements for the degree of
Master of Science
In Applied Earth Sciences: Petroleum Engineering

at the Delft University of Technology,
to be defended publicly on Tuesday December 21st, 2017 at 15:30 PM.

Supervisor:	Dr. D. Voskov	TU Delft
Thesis committee:	Prof. dr. W.R. Rossen,	TU Delft
	Dr. J.E.A. Storms	TU Delft

TU Delft

Author

Duaa Alshiroofi
d.alshiroofi@student.tudelft.nl
MSc Student, Petroleum Engineering & Geosciences
Department of Geosciences and Engineering
Delft University of Technology

Title

A multi-scale approach for numerical modelling of the subsurface CO_2 sequestration process.

Advisor

Dr. D.V. (Denis) Voskov
D.V.Voskov@tudelft.nl
Associate Professor
Department of Geosciences and Engineering
Delft University of Technology

Committee Member

Prof. Dr. W.R. (William) Rossen
W.R.Rossen@tudelft.nl
Head of Section, Professor of Reservoir Engineering
Department of Geosciences and Engineering
Delft University of Technology

Committee Member

Dr. J.E.A. (Joep) Storms
J.E.A.Storms@tudelft.nl
Associate Professor
Department of Geosciences and Engineering
Delft University of Technology

I

Acknowledgements

I would like to thank Dr. Denis Voskov for his extraordinary support in this thesis process. My words are coming short in describing my gratitude for your dedicated time, care and attention you put in, not only me, but all the other 12 students you have supervised the last year. You really are an inspiration. Even when you have to travel the world, go to Stanford because they need your brilliant mind there as well. Even then, you make sure I have everything I need to continue my thesis. And that is why I am where I am, my graduation.
It did not start well. You pushed and sometimes I wish you took all the reigns for a second, but you wouldn't. And looking back, I am happy you didn't. You patiently, quite tirelessly and firmly, - all of which are understatements for your continuous efforts - guided me with compassion and generosity.

I also want to thank Mark Khait. He implemented several formulas in C++ and helped me greatly. You are a very skilled coder, Mark!
Rahul Prabhakaran, you really deserve to be mentioned. We took some classes together and you were there at times where I just wanted to give up and punch the screen. You motivated me and helped me through it at the bad times. The times you cannot see the end of the thesis tunnel.

And finally, but most honorably, my family. My sisters and brother, Rusul, Fatima, Samer, you kept outstanding me even in my worst times. Even though you did not always stand behind my decisions, you motivated me in times that it was really tough to stay motivated. And my parents who have supported me in all of my choices and who have stood beside me. My mother, who would prepare my food. My father who I could bounce ideas off.

Thank you all, without you I would never made it to become a Petroleum Engineer!

II

Table of Content

III

List of Tables

IV

List of Figures

V

Nomeclature

V	Cell volume
Γ^{l}_{α}	Convective transmissibility in phase α
Θ^{l}_{α}	Diffusive transmissibility in phase α
$\Delta\Phi^{l}_{\alpha}$	Potential difference between control volumes (a and b) in phase α
p^{b}_{α}	Pore pressure in b in phase α
p^{a}_{α}	Pore pressure in a in phase α
p_e	Entry pressure
ρ_{α}	Density in phase α
ρ_c	Density of CO_2
ρ_w	Density of brine water
z^b	Height of b
z^a	Height of a
ΔX^{l}_{α}	Concentration difference between control volumes (a and b) in phase α
X^{b}_{α}	Concentration of b in phase α
X^{a}_{α}	Concentration of a in phase α
CFL_s	Total CFL
Δt	Time steps
A	Area
$\emptyset$	Porosity

Δx and Δz	Grid block sizes in x and z direction
Q_T	Total volumetric flow rate
$Q_{T,x}$	Total volumetric flow in x-direction
$Q_{T,z}$	Total volumetric flow in z-direction
K	Absolute permeability
g	Gravity
c_{max}	Maximum concentration at the solubility limit
μ	Viscosity
F	Dissolution rate
$\tilde{F}$	Dimensional dissolution rate
$\bar{F}$	Non-dimensional dissolution rate
h	Height of the single-phase brine region
(i,j)	Cell notation
l	length
u_α	Darcy's velocity in phase α
S_e	Effective saturation

1

Abstract

Subsurface carbon dioxide (CO_2) sequestration is a promising technology to reduce the CO_2 emission into the atmosphere. After injection into subsurface formation, the carbon dioxide plume can migrate several kilometres until it is fully trapped. Four major mechanisms play an important role in trapping which include structural trapping, residual trapping, dissolution trapping or mineralization. The accurate numerical simulation of the sequestration process is challenging owing to the complexity of buoyancy driven enhanced dissolution and convective propagation of the CO_2 plume. To resolve these processes, one often needs an extremely fine computational grid which makes the CPU time prohibitive for modelling at reservoir scale. Several simplified models were proposed which include analytical models (Hesse, 2008; Gasda et al., 2012), vertical equilibrium models (Gasda et al., 2012; (Pruess & Nordbotten, 2011) and an algebraic multi-scale model (Hesse, 2008).

Here we proposed and applied the multi-scale models with dissolution for modelling of CO_2 sequestration on the large-scale. Several numerical experiments are considered using adjusted small-scale simulation of the plume dynamic in a sloped aquifer. The enhanced rate of dissolution captured in the small-scale models with geometrical properties was then applied to the simulation in the realistic aquifer. A sink term applied at the CO_2-brine-interface is implemented in the ADGPRS program. This term numerically acts as the dissolution mass transfer that would otherwise occur in a compositional simulation at fine resolution.

It is important to contemplate the slow reduction in dissolution rate after the fingers begin to interact with the bottom of the reservoir. After interaction becomes significant, a reduction in the local dissolution rate is considered. We compared our multi-scale approach with a high-fidelity compositional simulation at high resolution, similar to the results presented in (Elenius, Voskov & Tchelepi, 2015). The applicability of the proposed approach was validated on the numerical model of a realistic aquifer.

2

Background and facts

There are many headlines lately in the news regarding the increase of carbon dioxide. This fact does something towards the goal of carbon emission. The main challenge in carbon dioxide sequestration is time, since there is a Paris climate goal of 2°C. Most International Energy Agency (IEA) and the Intergovernmental Panel on Climate Change (IPCC) requires widespread scenarios of Carbon Capture and Storage (CCS). The latest IEA requires 3800 megatons CCS per year. This is enormous compared to the dozens of megatons CCS stored nowadays. For example, the Sleipner side in Norway stores one megatons of CO_2 per year. The volume that must be stored in the ground each year is almost equivalent to the oil and gas volume extracted each year. In addition, it is possible to perform a mineral sequestration, ocean sequestration and geological sequestration. Ocean sequestration is a method in which CO_2 is injected into deep-sea waters; this is considered a high-risk operation (IPCC (2005)). Another option is to store CO_2 in depleted oil and gas reservoirs. However, the capacity of these reservoirs is limited. It has also been proposed to inject CO_2 into enhanced coal bed methane reservoirs, since this CO_2 can bind to coal. However, coal usually swells when it is filled with CO_2 which reduces the injectivity. The most visible option for sequestration is CO_2 injection into deep saline formations – underground layers of sandstone that are filled with salt water (brine). These formations have the largest capacity to store CO_2. Therefore, CO_2 sequestration into geological formations will be the focus of this thesis research. The questions, we are trying to answer here, are how much CO_2 can be stored (the capacity) and how safe is it (the leakage). Computer modelling will be an important resource to answer these questions.

3

Introduction

Carbon Dioxide (CO_2) storage or CO_2 sequestration is a method to reduce the concentration of CO_2 in the atmosphere by storing the CO_2 underground. The CO_2 can be injected into the saline aquifers. It will then dissolve in the brine which increases its density (McBride-Wright, Maitland, & Trusler, 2014). This introduces instability, which largely enhance CO_2 dissolution due to the natural convection (Rouhollah Farajzadeh, Salimi, Zitha, & Bruining, 2007; R. Farajzadeh, Zitha, & Bruining, 2009). The CO_2 dense brine will influence the viscosity of the brine and therefore it will sink towards the bottom of the reservoir (McBride-Wright et al., 2014). It is important to quantify the macroscopic CO_2 dissolution in brine to predict and to obtain the potential and long-term behaviour of CO_2 in aquifers (R. Farajzadeh et al., 2009). Since the dense CO_2 is sinking towards the bottom of the reservoir formation, the CO_2–rich brine is getting into contact with the fresh brine and the dissolution rate is accelerated. The increasing dissolution rate gives a shorter time scale for the storage for the gas by solubility trapping (McBride-Wright et al., 2014). Until now, the macroscopic dissolution trapping mechanism was studied under idealistic conditions of non-inclined reservoir (M. T. Elenius, Voskov, & Tchelepi, 2015). In this study, we focus on the dissolution rate for small-scale models at different inclinations to apply it for a simplified large-scale model.

3.1 Injection of CO_2

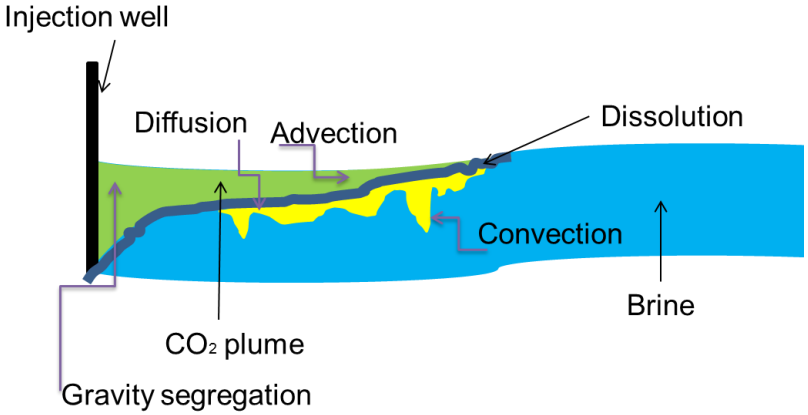

Figure 1: CO_2 injection and migration. The grey arrows show the direction, the black arrows show the meaning of the word.

Figure 1 shows how CO_2 is distributed in the aquifer. The CO_2 injection is through the vertical well in the left. The CO_2 is displacing the brine (the salty water already in place) and pushing it outwards following the pressure gradient. While the brine is displaced outwards, some of it is left due to the residual trapping. There is also a gravity force (CO_2 is lighter than water even if we inject it as supercritical form). Away from the injection well, the CO_2 plume flattens, and it forms a thin layer below the cap rock. Then it is moving along the cap rock, driven by gravity forces. The CO_2 will migrate until it becomes immobile.

3.2 Trapping Mechanism

The trapping mechanisms during and after CO_2 is injected into a geological formation varies a lot over time (Class et al., 2009). An illustration is given in Figure 2. Right after the injection, advection phenomena dominate the CO_2 spreading. Advection describes the movement of a quantity via the flow of a fluid, thus the movement of CO_2 into the brine, which is driven by viscous forces. The viscous forces arises due to the injection overpressure. Due to density differences between the CO_2 and the brine, advection is driven by buoyancy forces. After a while, advection slows down and is followed by an increase in dissolution of CO_2 into the brine (Class et al., 2009).

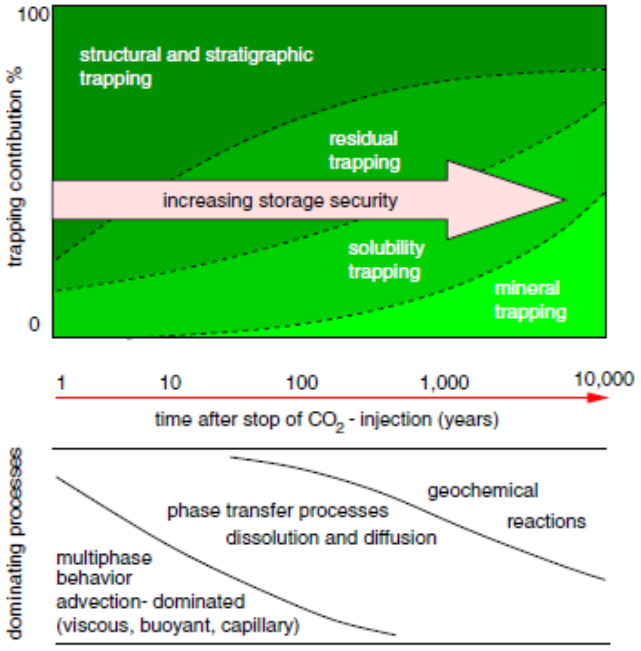

Figure 2: Variation of the trapping mechanisms and the dominant processes on different time scales from (Class et al., 2009; S. E. Gasda, Nordbotten, & Celia, 2012; Bert Metz, Ogunlade Davidson, HC De Coninck, Manuela Loos, & LA Meyer, 2005b).

The dominant trapping forces change over time. There are different trapping mechanisms known: geological/ structural trapping, residual trapping, solubility/ dissolution trapping, and mineral trapping (Bai, Wang, Fang, Zhang, & Song, 2014). To accurately estimate the amount for storage in realistic aquifers, numerical simulations are essential (Class et al., 2009).

3.2.1 Structural Trapping

Structural trapping is caused by very low flow velocity (Bachu, Gunter, & Perkins, 1994). When the buoyant CO_2 rises up in the aquifer, it will accumulate under the impermeable layer. A portion of the buoyant CO_2 is trapped in the pockets of the cap rock. Since it cannot move anymore, it will be permanently stored in the aquifer. The security of CO_2 storage increases with decreasing mobilization of CO_2. Therefore, the risk of leakage is being reduced (Shamshiri & Jafarpour, 2012).

3.2.2 Residual Trapping

The residual trapping is the most rapid method to remove CO_2 from its free phase. In fact, it is the CO_2, which was left behind, there where the mobile CO_2 has already passed. When the formation water intrudes the CO_2 plume then the CO_2 as residual gas is being trapped. (Ashcroft & Isa, 1997; Bai et al., 2014; Mo, Zweigel, Lindeberg, & Akervoll, 2005). When the CO_2 is displaced, the front and the tail of the CO_2 plume undergoes drainage and imbibition processes. Because of the imbibition process, residual gas is trapped in the rock pore spaces. This residually trapped gas becomes more significant with increasing the contact between the CO_2 plume and fresh parts of the aquifer. The residually trapped CO_2 will be eliminated over time because of dispersion, diffusion and dissolution (McPherson & Cole, 2000; Shamshiri & Jafarpour, 2012).

3.2.3 Dissolution Trapping

The density of the brine increases when CO_2 dissolves. This impedes the brine with dissolved CO_2 to sink downwards. Therefor there is no risk of CO_2 escaping from the surface anymore. How much of CO_2 will be soluble in the brine is a function of pressure, temperature and salinity. Buoyancy forces shows to limit the storage of free CO_2 but on the other hand it increases the solubility trapping by increasing the surface area of the contact between the CO_2 and the brine, which results in an enhanced dissolution (Shamshiri & Jafarpour, 2012).

3.2.4 Mineral Trapping

Mineral trapping is the safest way of storing CO_2, but at the same time, it is a slow mechanism for permanent storage. Based on chemical reactions between the CO_2 and the minerals, precipitation will take place. For mineral precipitation, the cations Ca^{2+}, Mg^{2+} and Fe^{2+} are necessary (Shamshiri & Jafarpour, 2012). The storage security is dependent on a combination of physical and geochemical trapping, it therefor increases from structural trapping, to residual trapping, to dissolution trapping, to mineral trapping (Rubin, 2006).

4

Physics

4.1 Physics of the plume migration

For this study, we inject supercritical CO_2 in a large-scale reservoir. The injected CO_2 will display the water first leaving some residual water behind. Both water and supercritical CO_2 are available in the system, therefore we have a two-phase system except a very close vicinity of the well where the CO_2 displaces and vaporize the water completely.

When CO_2 moves up, the water will move down because of the buoyancy forces. In addition, the difference in CO_2 concentration will create the diffusively driven dissolution, which force CO_2 to dissolve in brine. Due to the difference in density of brine, the brine with dissolved CO_2 will form unstable fingers and move down which brings more fresh brine up. This process can significantly enhance the macroscopic dissolution in comparison to purely diffusively driven processes. In addition, the capillary transient zone also plays an important role. When there is enough CO_2 on top of the brine, the volumetric distribution of CO_2 will follow the capillary pressure, constraint the gas phase distribution and form a capillary transient zone. At the interface of this zone, the gas saturation is equal to 0 and a pure brine phase is located below. However, the concentration of CO_2 in the brine phase is at CO_2 solubility limit. Once the dissolution process is started, the capillary transient zone become the source of the brine with high CO_2 concertation, which farther complicates the nonlinear dynamic of CO_2 (Elenius et al., 2014). The instability of the CO_2–rich brine on top of the aquifer layer increase a convection current. Brine without CO_2 is moving up to the interface while the CO_2-rich brine moves downwards. This accelerates the dissolution process, and hence the mass transfer rate. A constant CO_2 concentration is being obtained after a certain time of mixing in this system.

An example of this behaviour is shown in Figure 3. The gas saturation is shown for different times. The plume is migrating up-dip near the top of the permeable layer. It then keeps migrating under the sloping cap rock. The migration of the plume in the initial period is rapid because of the strong driving force (Pruess, 2011). The speed of the plume decreases when dissolution is taken into account, until it reaches a constant value after the transition period (Elenius, 2010). Subsequent advancement continues then with a constant speed. The plume is thinning out the further it migrates. Together with the out thinning plume, the mass flow of the CO_2 is decreasing with increasing distance of the original CO_2 emplacement.

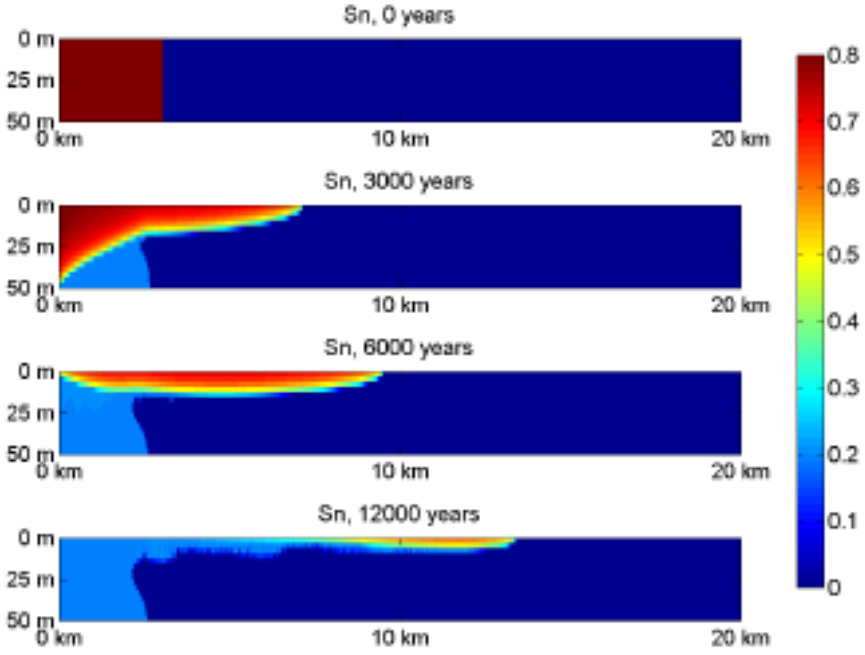

Figure 3: gas phase saturation with dissolution (from Elenius, 2010).

This behaviour is comparable with a model (Figure 4) introduced in Bickle et al. (2007), which shows the gravity driven flow of a less dense viscous fluid. This behaviour is similar to the behaviour of the CO_2 (density: 733 kg/m^3 and viscosity: 0.0611 cP, Nordbotton et al., 2011) in brine (density: 1099 kg/m^3 and viscosity: 0.511 cP, Nordbotton et al., 2011) shown in Figure 3.

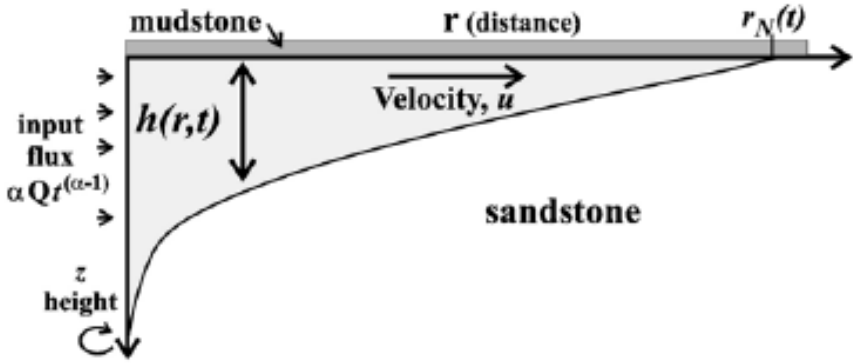

Figure 4: Illustration for a gravity driven flow of a less dense viscous fluid introduced along axis at t=0 into a porous medium initially filled with a fluid with a higher density ().

4.2 CO_2 Sequestration using ADGPRS

ADGPRS stands for Automatic Differentiation General Purpose Research Simulator, the simulation framework created at Stanford University for simulation of complex physics processes (Voskov & Tchelepi, 2012; Zaydullin et al., 2014; Garipov et al., 2016). It allows the flexible treatment of all nonlinear physics. In addition, it uses a spatial discretization that is second-order accurate for pressure. With this simulator numerical modelling of the CO_2 plume in a (non-) sloping aquifer with and without dissolution can be performed (Bickle, Chadwick, Huppert, Hallworth, & Lyle, 2007).

4.3 Objective paper

The accurate numerical simulation of the sequestration process is challenging owing to the complexity of buoyancy driven enhanced dissolution and convective propagation of the CO_2 plume. To resolve these processes, one often needs an extremely fine computational grid, which makes the CPU time prohibitive for modelling at reservoir scale. The objective of this paper is to apply and extend the multi-scale application for modelling of CO_2 sequestration on the large-scale. Several numerical experiments are considered using adjusted small-scale simulation of the plume dynamic in a sloped aquifer. Limitations in previous studies are that there was no real multiscale implementation applied, there were also no changes in inclination taken into account, and there was a mismatch between results from large and small-scale local dissolution which might be explained by absence of inclination in the small-scale models (Johnson, Nitao, Steefel, and Knauss (2001).

Therefore, for this study, the enhanced rate of dissolution will be captured in the small-scale models with geometrical properties and will be applied to the simulation in the realistic aquifer. A sink term is implemented in the ADGPRS program to be applied to the CO_2-brine-interface. This term numerically acts as the dissolution mass transfer that would otherwise occur in a compositional simulation at fine resolution. The applicability of this approach will then be validated on the numerical model of a realistic aquifer; namely the Johansen formation (Eigestad et al., 2009).

5

Problem definition

Until now, the small-scale models are studied under idealistic conditions of non-inclined reservoir (M. T. Elenius et al., 2015). In this study, we focus on the dissolution rate for small-scale models at different inclinations to apply it for a simplified large-scale model. The equations used to describe two-phase flow and transport are shown in this section.

5.1 Methodology

The problem is modelled as a two-component, two-phase, compositional problem. CO_2 exists only in the gaseous phase, brine exists only in the aqueous phase, therefore components, and phases are the same in the mass conservation equation.

5.1.1 Mass Conservation

The mass conservation equation in phase "α" is (1):

$$\frac{\partial}{\partial t}\sum_{\alpha}(\emptyset\rho_{\alpha}S_{\alpha}X_{\alpha}) + \nabla .\sum_{\alpha}(\rho_{\alpha}X_{\alpha}u_{\alpha} + S_{\alpha}\rho_{\alpha}J_{\alpha}) = 0 \tag{1}$$

In which the $\emptyset$ is the porosity, $\rho_{\alpha}S_{\alpha}$ denote respectively densities and saturations. X_{α} denotes mass fraction of supercritical CO_2. The Darcy velocities, u_{α}, and the Fick's diffusion flux, J, are given by (2):

$$u_{\alpha} = -\frac{k_{r\alpha}k}{\mu_{\alpha}}(\nabla p_{\alpha} - \rho_{\alpha}g) \quad , \quad J_{\alpha} = -\emptyset D_{\alpha}\nabla X_{\alpha} \tag{2}$$

In which k is the absolute permeability, k_r is the relative permeability, μ_{α} is the viscosity, p_{α} is the phase pressure, D_{α} is the diffusion coefficient and g is the gravitational acceleration. The relative permeability's and the phase saturations, with an associated capillary pressure were then calculated using the following equations. These are the rock-fluid properties.

$$1 = \quad S_w + S_g \tag{3}$$

$$S_e = \frac{S_w - S_{wr}}{1 - S_{wr}} \tag{4}$$

$$k_{rw} = S_e^4 \tag{5}$$

$$k_{rn} = 0.4\,(1 - S_e^2)(1 - S_e)^2 - C \tag{6}$$

$$p_c = \frac{p_e}{\sqrt{S_e}} = \frac{0.2}{\sqrt{S_e}} = p_n - p_w \tag{7}$$

S_e in equation 3 is the effective water saturation and C in equation 5 is a constant value. This constant value can be calculated from k_{rn}=0 at S_n=S_{nr} using equation 5, since hysteresis is not modelled for this study. From M. T. Elenius et al. (2015) a number for the constant variable was obtained: C = 0.011. Residual trapping is modelled using only drainage functions. To avoid pressures tending to infinity, S_e = 10^{-3} was used instead of S_e <10^{-3}. Since the phase densities differ and the capillary pressure is related to the saturation, a so-called capillary transition zone (CTZ) develops in the plume, where the CO_2 phase saturation in the plume increases with height above the single-phase brine region. The entry pressure, p_e, was taken to be 20 kPa from M. T. Elenius et al. (2015) All the used parameters including the values are described in **Fout! Verwijzingsbron niet gevonden.** (M. T. Elenius et al., 2015), with most of them a re adapted from Dahle, Eigestad, Nordbotten, and Pruess (2009).

Table 1: Fluid and Reservoir Properties adapted from (M. Elenius et al., 2010).

Parameter	Value
Absolute Permeability, k	100 md
Porosity, ∅	0.15
Viscosity of water phase, μ_w	0.511 cP
Viscosity of gaseous phase, μ_g	0.35 cP
Density of water phase, ρ_w	1033 kg/m^3
Density of gaseous phase, ρ_g	733 kg/m^3
Irreducible water phase saturation, S_{wt}	0.20
Residual gaseous phase saturation, S_{sn}	0.20
Acceleration due to gravity, g	9.81 m/s^2
Molecular diffusion coefficient, D	2x 10^{-9} m^2/day

5.1.2 Convection

The interaction of the CO_2 phase with the brine phase is based on convection phenomena. Convection is the collective motion of particles in a fluid and encompasses both diffusion and advection. The advection is the motion of particles along the bulk flow, while diffusion is the net movement of particles from high concentration to low concentration. The advection equation for 2D in Cartesian coordinates is:

$$u.\nabla = u_\alpha \frac{\partial}{\partial x} + u_z \frac{\partial}{\partial z} \tag{7}$$

Where $u = (u_\alpha,\ u_z)$ is the velocity field. For a conserved quantity the advection equation described by a scalar field, ψ, is expressed by a continuity equation. The partial differential equations for advection and diffusion are shown below.

$$\frac{\partial \psi}{\partial t} + \nabla . (u_\alpha \psi) = 0 \ \ (advection) \tag{8}$$

$$\frac{\partial \psi}{\partial t} = \nabla . (D \nabla \psi) \ \ (diffusion) \tag{9}$$

Here ψ is the quantity in consideration; u is the fluid velocity and D the diffusion coefficient.

5.1.3 Numerical treatment

ADGPRS allows for flexible treatment of highly nonlinear physics and different formulations that are implemented in a single simulation framework. For this work Fully Implicit Method for approximation in time was used. All the nonlinear unknowns are taken at the new time step (n+1). The discrete form of the equation can be rewritten as follow.

For the components, H_2O and CO_2, the mass conservation equation in discrete form is shown in equation (10). Each component can exist in both, wetting phase and non-wetting phase.

$$V[(\sum_\alpha \Phi S_\propto \rho_\alpha X_\alpha)^{n+1} - (\sum_\alpha \Phi S_\propto \rho_\alpha X_\alpha)^n] - \sum_l \left[\sum_\alpha \left((\rho_\alpha X_\alpha \Gamma_\alpha)^l \Delta\Phi_\alpha^l + (\rho_\alpha \Theta_\alpha)^l \Delta X_\alpha^l\right)^{n+1}\right] = 0 \quad (10)$$

V = V(x,y,z) – cell volume

$\Gamma^l_\alpha = T^l_\gamma k^l_r/\mu^l_\alpha$ – convective transmissibility

$\Theta^l_\alpha = T^l_\Theta S_\alpha$ – diffusive transmissibility

T^l_Θ and T^l_γ – constant part of transmissibility (depends on spatial discretization). Where l is the interface.

$\Delta\Phi_\alpha^l = p_\alpha^{n+1} - p_\alpha^n - \rho_\alpha g(z^{n+1} - z^n)$ – Difference in potential between control-volumes n+1 and n (in where p is the pore pressure)

$\Delta X_\alpha^l = X_\alpha^{n+1} - X_\alpha^n$ – Difference in concentration between control volumes n+1 and n.

This formula was discretised to be implemented in ADGPRS:

$$V\left[\left(\sum_{\alpha}\Phi S_{\propto}\rho_{\alpha}X_{\alpha}\right)^{n+1}-\left(\sum_{\alpha}\Phi S_{\propto}\rho_{\alpha}X_{\alpha}\right)^{n}\right]$$
$$-\left[\sum_{\alpha}\left(\left(\rho_{\alpha}X_{\alpha}\frac{T_{\gamma}^{i+\frac{1}{2},j}\,k_{r}^{i+\frac{1}{2},j}}{\mu_{\alpha}^{l}}\right)^{i+\frac{1}{2},j}\left(p_{\alpha}^{i+1}-p_{\alpha}^{i}-\rho_{\alpha}g(z^{i+1}-z^{i})\right)\right)\right.$$
$$-\left(\left(\rho_{\alpha}X_{\alpha}\frac{T_{\gamma}^{i-\frac{1}{2},j}\,k_{r}^{i-\frac{1}{2},j}}{\mu_{\alpha}^{l-1}}\right)^{i-\frac{1}{2},j}\left(p_{\alpha}^{i}-p_{\alpha}^{i-1}-\rho_{\alpha}g(z^{i}-z^{i-1})\right)\right)$$
$$+\left(\left(\left(\rho_{\alpha}\,T_{\theta}^{i+\frac{1}{2},j}S_{\alpha}\right)^{i+\frac{1}{2},j}(X_{\alpha}^{i+1}-X_{\alpha}^{i})\right)-\left(\left(\rho_{\alpha}\,T_{\theta}^{i-\frac{1}{2},j}S_{\alpha}\right)^{i-\frac{1}{2},j}(X_{\alpha}^{i}-X_{\alpha}^{i-1})\right)\right)$$
$$+\left(\left(\rho_{\alpha}X_{\alpha}\frac{T_{\gamma}^{i,j+\frac{1}{2}}\,k_{r}^{i,j+\frac{1}{2}}}{\mu_{\alpha}^{l}}\right)^{i,j+\frac{1}{2}}\left(p_{\alpha}^{i+1}-p_{\alpha}^{i}-\rho_{\alpha}g(z^{i+1}-z^{i})\right)\right)$$
$$-\left(\left(\rho_{\alpha}X_{\alpha}\frac{T_{\gamma}^{i,j-\frac{1}{2}}\,k_{r}^{i,j-\frac{1}{2}}}{\mu_{\alpha}^{l-1}}\right)^{i,j-\frac{1}{2}}\left(p_{\alpha}^{i}-p_{\alpha}^{i-1}-\rho_{\alpha}g(z^{i}-z^{i-1})\right)\right)$$
$$\left.+\left(\left(\left(\rho_{\alpha}\,T_{\theta}^{i,j+\frac{1}{2}}S_{\alpha}\right)^{i,j+\frac{1}{2}}(X_{\alpha}^{i+1}-X_{\alpha}^{i})\right)-\left(\left(\rho_{\alpha}\,T_{\theta}^{i,j-\frac{1}{2}}S_{\alpha}\right)^{i,j-\frac{1}{2}}(X_{\alpha}^{i}-X_{\alpha}^{i-1})\right)\right)\right]$$
$$=R_{i}^{\cup}$$

In which 'i,j' is the center of control volume (Figure 5). The black part of the formula represents the accumulation, the red part represents the advection and the blue part represents the diffusion term. The resident brine is the wetting phase and the supercritical CO_2 is the non-wetting phase (also referred to as the water and gaseous phases). The conservation equation is for brine and CO_2. We will ignore the dependency of ρ on composition, because there is no composition right now. But the reason that we get the fingering effect is mainly based on the ρ (which is a function of X). Now we will ignore the effects of ρ. Instead we will say that we have a rate estimated on the small-scale model. This will be the rate of dissolution. We use a new equation in which the density is only a function of pressure. The rate of dissolution will be distracted, this we will call a sink term. A small CO_2 compressibility (10^{-7} 1/bar) was introduced to avoid numerical issues. For the small-scale simulations, the time-step size was limited by $\Delta t_{max} = 10$ days, which produced small time-truncation error and quadratic convergence of the nonlinear solver for the finest resolution for our test cases. For the large-scale simulations the time step

was limited by $\Delta t_{max} = 100\ days$.

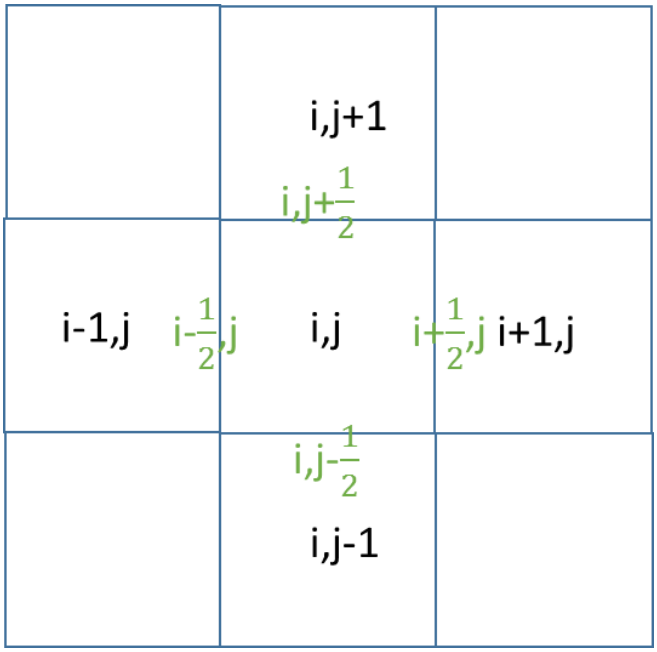

Figure 5: center of control volume i,j and cells around.

5.2 Calculation dissolution rate model

The non-dimensional dissolution rate is approximated by using the following formula. This formula is an average taken within the convective regime from Szulczewski et al. (2013):

$$\bar{F} = -0.011 \log d + 0.016 \tag{11}$$

Small d's are obtained for aquifers with large absolute permeability. Based on the approximations of Elenius et al. (2014) a 'd' of 0.0258 was used. When the relative permeability is very small (k_r=0.001) the value of d increases with a factor bigger than 10. The dissolution rate will then be enhanced. This is based on the simplified linear stability analysis which can be made using the model $k_r = e^{dz_n}$. Where negative z_n is the non-dimensional distance above the interface (Maria T. Elenius et al., 2014).

$$z_n = \frac{zK\Delta\rho_w g}{D\emptyset\mu} \tag{12}$$

In the non-dimensional setting, the critical wavelength is a function of k_r only, i.e., it is not dependent on the absolute permeability and so on (M. T. Elenius et al., 2015). From here, also the dimensional dissolution rate can be calculated by multiplying the equation (11) as follows:

$$\tilde{F} = \bar{F} * K\Delta\rho_c\, g \frac{c_{max}}{\mu} \tag{13}$$

Where K is the absolute permeability, ρ_c is the density of CO_2, g is the gravity, c_{max} is the concentration

at the solubility limit and μ is the viscosity. The dimensional dissolution rate of CO_2 is the mass of CO_2 dissolved per year and square meter of the interface (Maria T. Elenius et al., 2014).

$$\tilde{F} = \overline{(F} * K\Delta\rho_c \, g\frac{c_{max}}{\mu})/ \, ((\frac{1}{365})/(3600 * 24)) \tag{14}$$

This model is shown in all the plots with a dotted line with a horizontal start until ~350 years (also called t_{peel}) and then it starts to decrease linearly.
The dissolution rate calculated for all the different situations is obtained from the rate at which CO_2 enters the single-phase brine region (M. T. Elenius et al., 2015):

$$F = h\emptyset\frac{\partial\bar{c}}{\partial t} \tag{15}$$

This h represents the height of the single-phase brine region, which is 50m for this research.

5.3 Test case description small-scale model

First we use a small-scale model with dimensions: 400m x 50m. The CO_2 on top of the reservoir is separated from the brine below. Across the interface, CO_2 will dissolve into brine to form a diffusive boundary layer that grows with time (M. Elenius, Tchelep, & Johannsen, 2010). Each meter on the left and right boundary, represent a buffer. The model is studied for different inclinations. The results are needed for the large-scale model (20km x 50m) later in this research. The model sketch in Figure 1Figure 6 contains a sealed-sides boundary condition, which tends to bias the estimated effective permeability toward a low value. This is because it consistently underestimates the reservoir flow characteristics by thickening shale barriers and narrowing sand channels (King, MacDonald, Todd, & Leung, 1998; Nordbotten & Dahle, 2011). The buffer (large boundaries) on both sides of the reservoir mimic in constant pressure. Physically they behave like a Dirichlet boundary condition. The top and bottom boundaries are Neumann boundary conditions and they are no flux boundary. The CO_2 is provided by the initial conditions, which features a CTZ with dissolved CO_2 at the solubility limit. The small vertical flux induced by convection has negligible impact on the saturation distribution. When the CO_2 dissolves the interface recedes. This behaviour also occurs in large-scale plume migration as brine imbibes into the trailing part of the plume, and CO_2 gets residually trapped.

5.3.1 Initial and boundary conditions small-scale

A 2D idealized initial condition is shown in Figure 6. The top, left and right surface are no-flow boundaries, while the bottom is an open-boundary condition. The aquifers inclination is changeable and is set to be 0° - 9°. The CO_2-saturated region will be initialized at irreducible water saturation $S_w=S_{wt}$, and the rest of the domain will be at $S_w=1$.

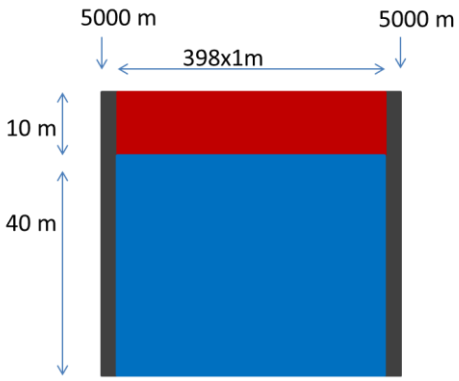

Figure 6: Sketch of the CO_2 sequestration process in a simple geometry. A CO_2 gas phase accumulates along the impermeable top boundary. It slowly dissolves into the underlying brine, forming a heavier boundary layer. The resulting gravitational instability leads to the convective transport of CO_2-saturated brine plumes (Riaz, Hesse, Tchelepi, & Orr, 2006). The porosity is 0.15 everywhere, the boundaries of 5000m represents the buffer. The red area (height of 10m) shows the CO_2 part, while the blue area (height of 40m) shows the brine part. The total length of the small-scale model is 400m. The model will be used for varying inclinations.

5.4 Test case description large-scale model

The large-scale problem is inspired by the benchmark proposed by Riaz et al. (2006) and Dahle et al. (2009). Some parameters that were not defined in the benchmark are chosen based on M. T. Elenius et al. (2015) and Dahle et al. (2009). The depth of the lowest point of the domain in the large-scale is 3025m and the highest point is 2675m. These depths are only important for the choices of density and solubility. All the boundaries are closed to flow, apart from the right boundary (Figure 7).

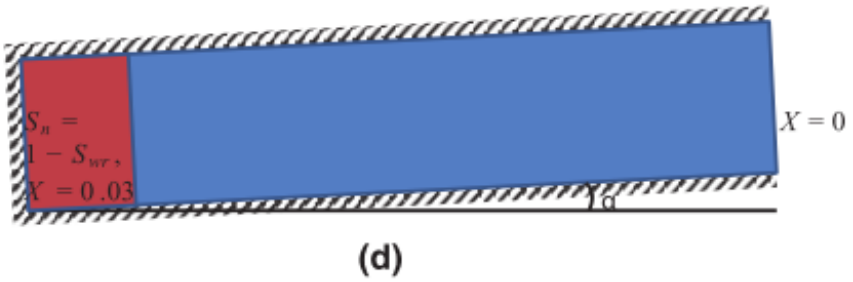

Figure 7: Aquifer with slope in which apart from the right boundary, the boundaries are closed to flow.

At initial hydrostatic pressure the right (blue) part in Figure 7 has a single-phase brine. This model is much simplified mainly to obtain a well-defined problem. The length of the domain is 20.000 meters from which 1200 meter is the initial CO_2 region as given by King and Mansfield (1999). This corresponds to approximately one fourth of the injected CO_2 mass in the previous benchmark (Nordbotten & Dahle, 2011). The CO_2 is placed in the down-dip part of the aquifer such that only residual brine (saturation 0.2) is present there. The simplified initial plume geometry, as used here, cannot produce realistic early plume migration, but is motivated by our focus on the post-injection period.

6

Results & Discussion

Small-scale

6.1 Sensitivity study

To obtain a saturation profile, an immiscible two-phase simulation was conducted. Different grid resolutions were used and are shown in Table 2. A sensitivity analysis was done to examine the effect of spatial resolution on the position of the CO_2 plume. The horizontal domain (length) was truncated at 400m. The aspect ratio was not kept constant for the vertical and horizontal grid resolutions. The finest resolution used was 0.5m x 1.0m and the largest was 2.0m x 1.0m. The computational run time significantly increased as finer resolution were used. The CFL (Courant, Friedrichs, Lewy) number characterizes the throughput quantity for each cell. The summation for the total CFL (CFL_s) is based on the CFL number in x and z (CFL_x, CFL_z), this is given in equation 16. In which Δt is the time step, A is the area, $\emptyset$ is the porosity. Gridblock sizes are Δx and Δz in the x and z direction. Q_T is the total volumetric flow rate with the constituent flow rates $Q_{T,x}$ and $Q_{T,z}$ in the x and z direction.

$$CFL_s = CFL_{S,x} + CFL_{S,z} = \frac{Q_{T,x}\Delta t}{A_x \Delta x \emptyset}\frac{df_g}{dS_g} + \frac{Q_{T,z}\Delta t}{A_y \Delta z \emptyset}\frac{df_g}{dS_g} \tag{16}$$

This equation can then be simplified to:

$$CFL_s = \frac{Q_T \Delta t}{V\emptyset}\frac{df_g}{dS_g} \tag{17}$$

In Table 2 the averaged maximum CFL by time steps is shown for the different grid resolutions. The lower the CFL indicates that the nonlinear solution is more stable. Higher CFL numbers can imply a computationally expensive approach when nonlinear solver may require more iterations. The finer the grid resolutions (spatial discretization) gave a higher CFL number. This reflected the run times. The higher the CFL averages by time steps has a bigger amount of number of blocks and a higher run time in days, but a smaller DX value. Figure 8 illustrates the results of the sensitivity study. From Figure 8 it is clear that the coarser the resolution is, the shorter plume advancement is yielded. Coarser grid blocks require more time (Table 2).

Table 2: Spatial discretization and run times. Also the maximum CFL averaged by time steps is recorded.

DX	DZ	Run time in hours	Number of blocks	MaxCFL averaged by time steps
0.5	1	26.5	40000	2.864
1	1	13.4	20000	1.431
1.25	1	12.3	16000	1.144
2	1	7.4	10000	0.714

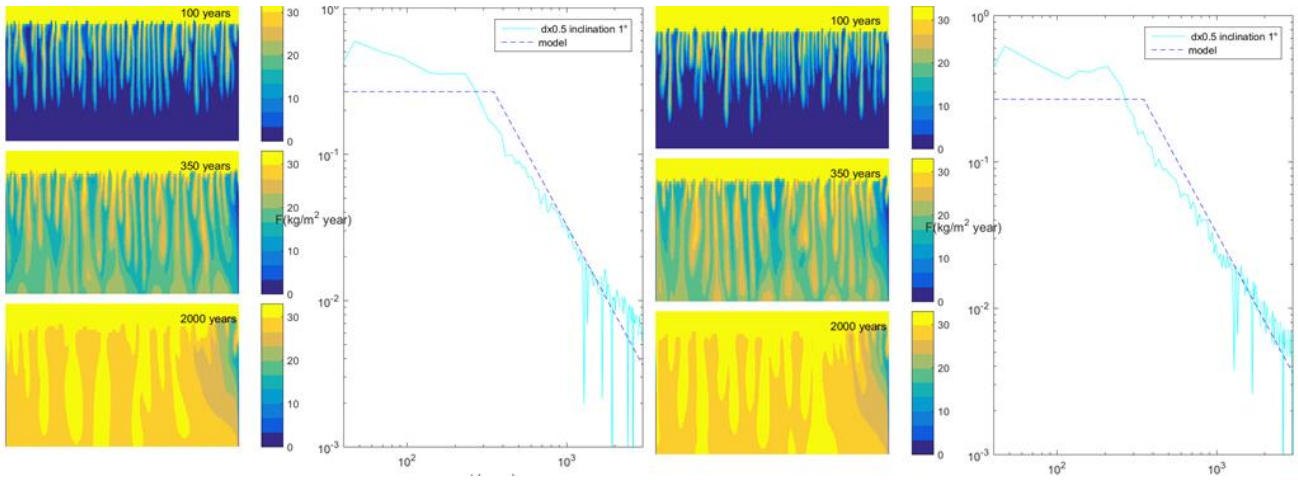

Figure 8: coarser resolutions yield shorter plume advancement and lower amounts of CO2 in mobile blocks at detachment time. The left picture represents a 1° inclined model with dx 1.0 and the right one represents a 1° inclined model with dx 0.5.

Table 3 summarizes the grid block sizes used. We tried different domain dimensions, but because of stability issues we decided to continue with a domain were the vertical dimension is 50m and the horizontal dimension is 400m (red box in Table 3

Table 2). The maximum time step was kept constant at 10 days. The smaller the DX the more simulation time is needed to run it (Figure 11), but the more accurate the results are. For the model with NX400 and NZ50 the inclinations 0°-9° are shown for dx=0.5 (Figure 10) and dx=1 (Figure 9). The start seems to be similar for both dx=0.5 and dx=1.0, but the accuracy after 1000 years is better for dx=0.5 (Figure 10). However, the results are affected by instability of the physical process

Table 3: Spatial discretization for compositional simulations for an inclination of 1°.

DX	DZ	NX	NZ	Number of blocks
1	1	100	50	5000
1	1	200	50	10000
1	1	50	50	2500
1	1	400	50	20000
0.5	1	400	50	20000
1	1	800	50	40000

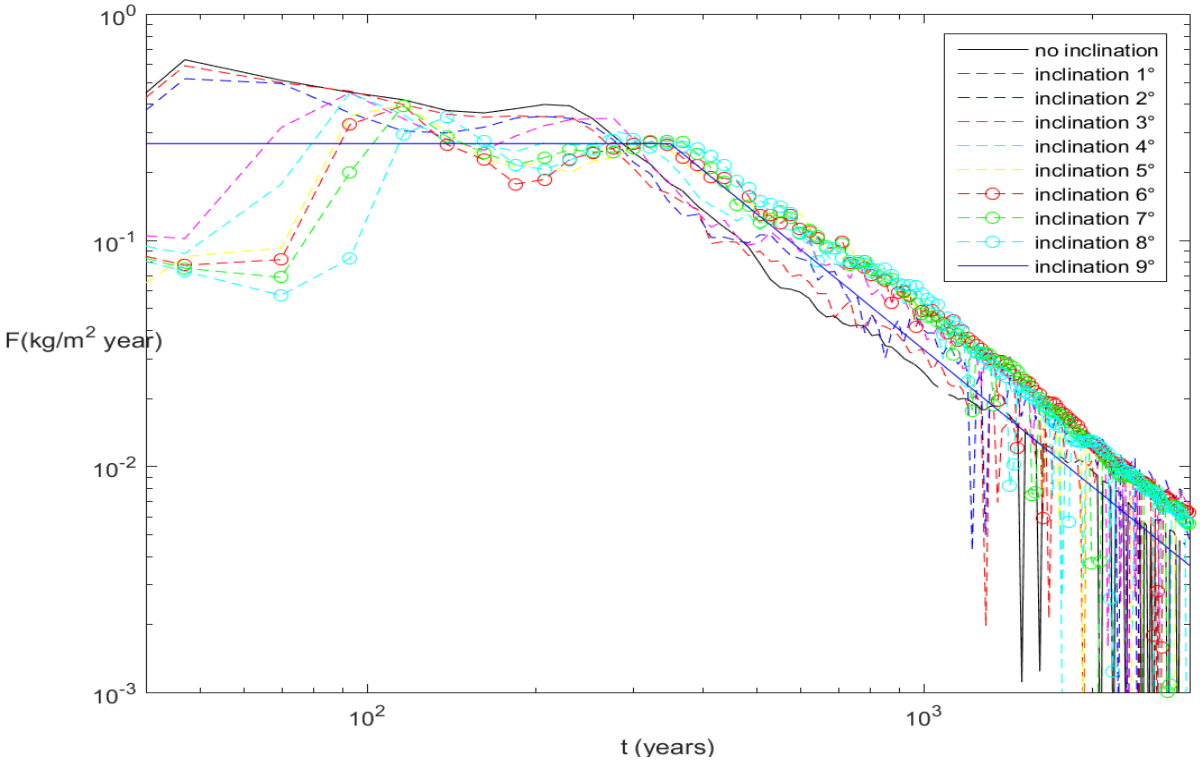

Figure 9: Dissolution rate for small-scale model. For dx = 1 and inclinations 0-9°.

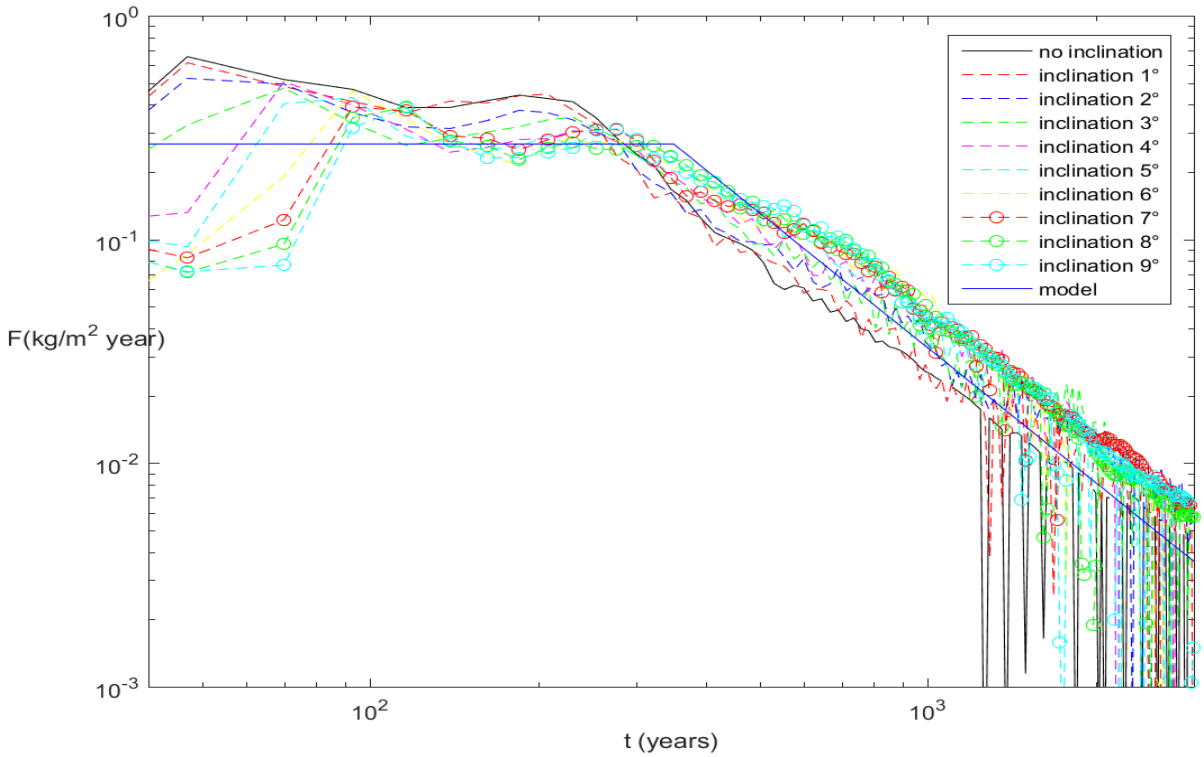

Figure 10: Dissolution rate for small-scale model. For dx = 0.5 and inclinations 0°-9°.

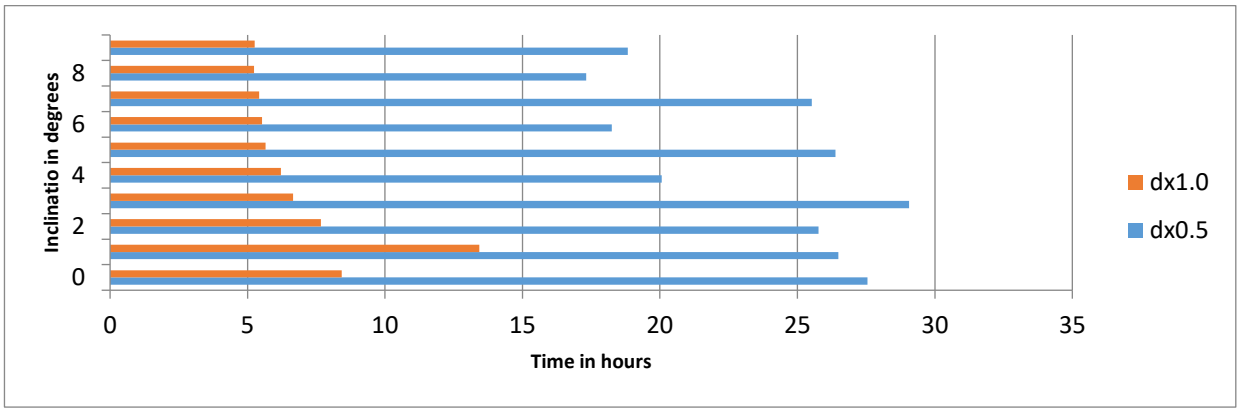

Figure 11: Running time in hours for grid block inclination of 0°-9° and dx0.5 vs dx1.

6.2 Numerical instabilities

The diffusion of CO_2 into underlying formation waters increases the density of water near the top of the aquifer, bringing the system to a hydro-dynamically unstable state. Instabilities can cause convective mixing and greatly accelerates the dissolution of CO_2 into the aquifer. Accurate estimation of the rate of dissolution is important for risk assessments because the timescale for dissolution is the timescale over which the CO_2 has a chance to leak through the cap rock or any imperfectly sealed wells (Dahle et al., 2009). For that, we analysed the convective mixing in the small domains to use the knowledge later for the large-scale plume migration. From results of Hassanzadeh, Pooladi-Darvish, and Keith (2005) it is clear that complete dissolution of CO_2 in the aquifer by pure diffusion will take thousands of years, whereas this time is much smaller in the presence of convective mixing. The presence of convective mixing dissolves the aquifer more than 60% of its ultimate dissolution rate. Pressure at the boundary drops slightly with time during the diffusion period. Due to the action of convection mixing there is a sharp pressure drop which dissolves a large volume of CO_2 into the aquifer (Hassanzadeh et al., 2005).

In order to examine the role of numerical instabilities on the plume migration, simulations were performed using different numbers of grid blocks. The dissolution rate for a domain with 50x50 grid blocks which includes a buffer from each side is compared with the dissolution rates of a 100x50 grid blocks for two different resolutions and with 200 x 50, 400 x 50 and 800 x 50. The combinations are shown in Table 4: . In addition, the run time for these combinations is shown (Table 5 & Figure 12).

Table 4: Combinations for the numerical instability.

Length (m)	Height (m)	Resolution
50	50	1
50	50	0.5
100	50	1
100	50	0.5
200	50	1
200	50	0.5
400	50	1
400	50	0.5
800	50	1

Table 5: Run time in days for the combination for numerical instabilities from Table 4.

Length(m) x Height(m)	inclination 1		No inclination
	dx0.5	dx1	dx1
50x50	2.7	3.6	1.4
100x50	4.5	9.6	2.4
200x50	8.2	10.2	4.6
400x50	26.5	13.4	8.4
800x50	-	13.6	15.0

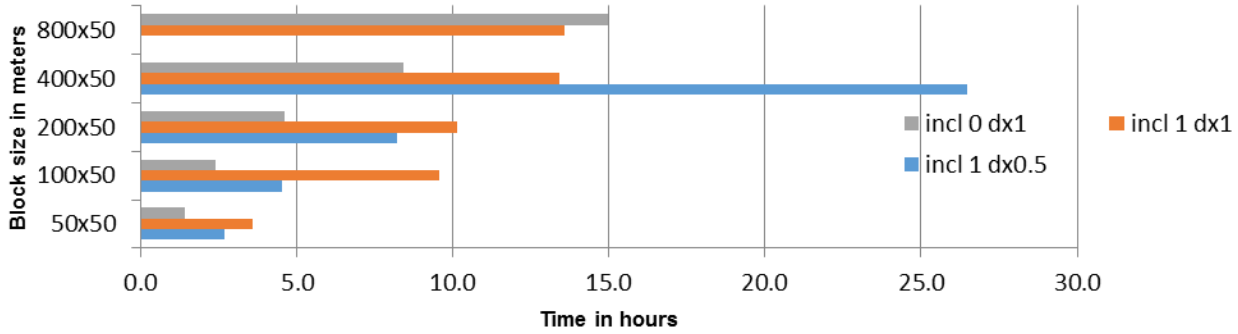

Figure 12: running time for different blocksizes.

Increasing the grid blocks from 50m x 50m, to 100m x 50m, to 200m x 50m, to 400m x 50m and to 800m x 50m (Figure 13) shows a more similar behaviour for the dissolution rate when comparing the inclined and not inclined grid block with each other. The inclined model shows a dissolution rate behaviour which is closer to the analytical model (baseline) (Figure 13). When changing the grid-block resolution from 1.0 to 0.5 (Figure 13), the accuracy changes a lot for the inclined block and therefor the similarity of the dissolution rate decreases and becomes less stable over time. The solubility of CO_2 in brine decreases with increasing pressure, decreasing temperature and increasing salinity (Hassanzadeh et al., 2005).
The homogenous model utilized allows numerical instabilities for the initiation of gravity fingers. The accuracy increases with an increased length of the domain. The larger the length is, the bigger the comparison is between a non-inclined and an inclined block as is shown in Figure 13C compared to Figure 13A. The larger the inclination is the shorter is the running time. An increased inclination shows a steeper grid block. The pressure difference is higher between the top right block, and the bottom left block. Therefor the gravity fingers of the CO_2 dissolves into the underlying brine which grows faster in time compared to a smaller inclination. The plume moves quicker and needs less running time compared to a lower pressure difference (and a lower inclination). This is not applicable for a grid block size of dx0.5. The smaller the grid block size is, the more accurate the results are, but the faster they are being influenced and therefor do not follow the same behaviour of a grid size of dx 1.0, as shown in Figure 11. The inclination factor is not the dependent variable in this case. The needed time is inconsistent for the different inclinations.

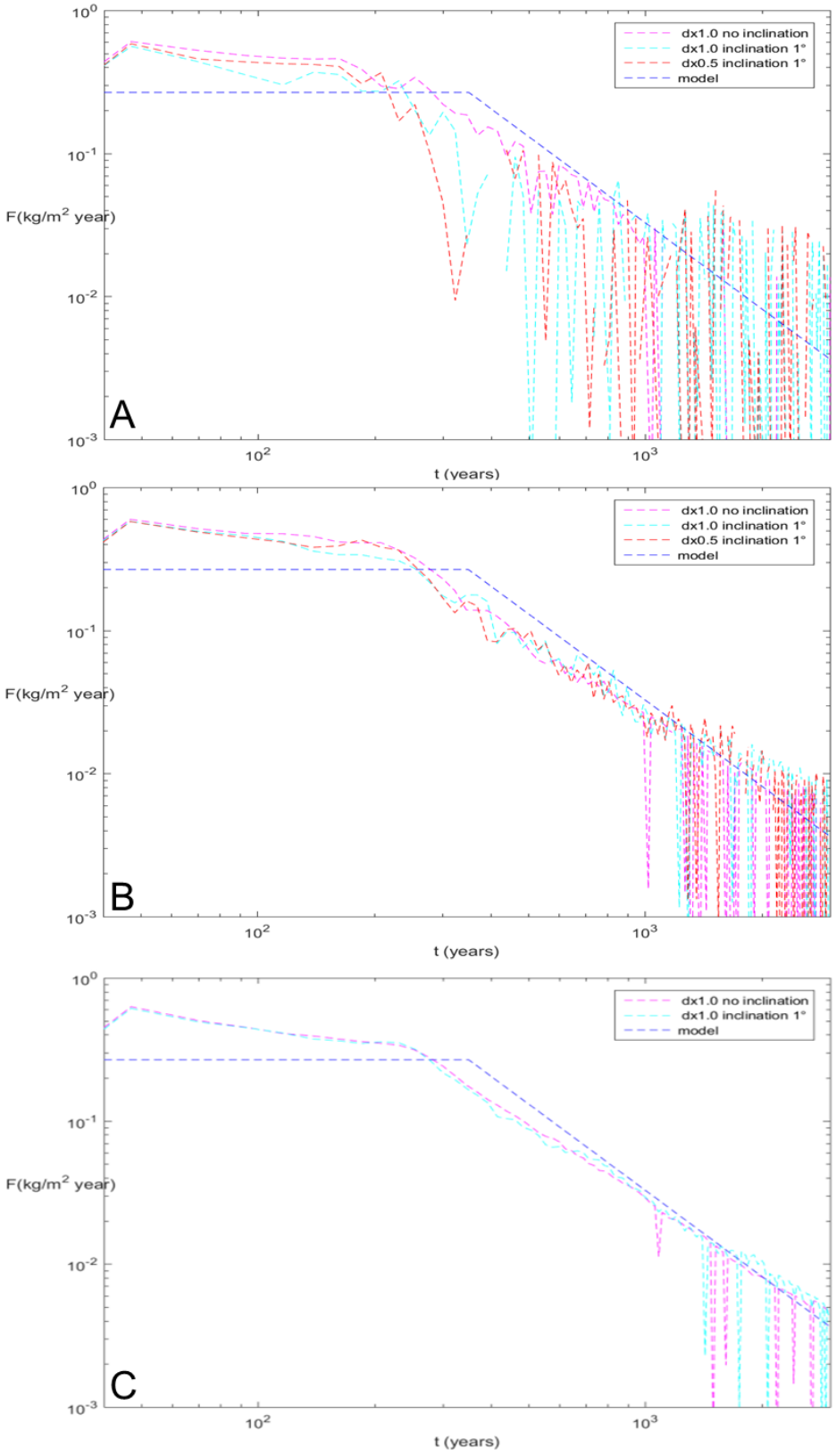

Figure 13: Dissolution rate (kg/m2 year) in a 50 x 50 m domain (A), 200 x 50 m domain (B) and 800 x 50 m domain (C) with a stagnant CTZ. For an inclination of 1° with dx1.0 and dx0.5. In addition, non-inclined version with dx 1.0 was compared to the baseline.

6.3 Dissolution rate

For CO_2 sequestration, structural and stratigraphic traps are the most attractive because of their low permeability seal, which makes upward migration of CO_2 harder. Therefor the risk of leakage of CO_2 to the surface is reduced but not eliminated (Metz et al., 2005b; Szulczewski, Hesse, & Juanes, 2013). However, during early times the CO_2 phase rises toward the cap rock, therefor residually trapped CO_2 will be left behind (Bert Metz, Ogunlade Davidson, Heleen De Coninck, Manuela Loos, & Leo Meyer, 2005a). CO_2, when injected in the ground, will dissolute into the groundwater. Dissolution of CO_2 will eliminate the risk of CO_2 leakage more. CO_2 has a molecular weight of 44kg/mol versus a molecular weight of 18kg/mol for water vapour, under the same conditions. Therefor when CO_2 dissolves with the water it will be denser than the groundwater itself, therefor it will cause some gravitational instability. This will express itself in being unstable and therefor it breaks up into descending fingers of denser brine. These will prefer to sink rather than go upwards through a leakage pathway (M. T. Elenius et al., 2015; Riaz et al., 2006; Szulczewski et al., 2013; Xu, Chen, & Zhang, 2006). If a porous layer is just below the CO_2-brine interface, the dissolution of CO_2 will initially occur via diffusion only. Diffusion in physics, describes the behaviour of the motion of particles in a material resulting from the random movement of each particle. This would lead to a diffuse boundary layer of CO_2-rich fluid below the top boundary. The mass simultaneously rise upwards while the fingers are going downwards. The upward going fluid leads to a sharp concentration gradients at the top boundary that increases the dissolution (Xu et al., 2006). When the fingers reach the bottom of the reservoir, the dissolved CO_2 starts to circulate back (Figure 14). The back circulated CO_2 lowers the concentration gradient which makes the dissolution rate continually decrease (Figure 15) (Szulczewski et al., 2013). Besides the distribution of CO_2 into the aquifer by diffusion, convective mixing plays also an important role for enhancing the dissolution rate. The dissolution rate is defined as the amount in kilograms of CO_2 mass transferred to the single phase brine region across the interface (Metz et al., 2005a; Szulczewski et al., 2013). The convective mixing plays a role in increasing the density of the brine when the CO_2 is dissolved into it (M. T. Elenius et al., 2015). At the local minimum of the dissolution mass rate plot is the onset of convectively enhanced dissolution. The onset describes the beginning of the interactive effects of dissolution, diffusion and convection phenomena. Without dissolution, diffusion and convection, the dissolution rate would monotonically decrease because dissolution would have occurred by molecular diffusion only (S. Gasda, Nordbotten, & Celia, 2011). When the fingers descend, the concentration gradient across the two-phase interface gradually decreases with time (Figure 14), and this decreases the diffusion/dissolution rate (Figure 15). At the onset of convectively enhanced dissolution, the creation of gravity fingers allowed for the increase in the dissolution rate (Figure 15). Further instabilities and interaction between fingers caused some fluctuation in the dissolution rate (Figure 15). As time progressed, the fingers moved away from the interface, where the density constant irrespective of its changes in form in this closed system. This is due to the conservation of mass. Consequently, the dissolution rate proportionally decreases (Pruess & Nordbotten, 2011). The fingering effect and dissolution rate was then also observed for different heights. In Figure 15, the sensitivity of the height is shown. The smaller the height, the earlier the fingers reach the bottom, the faster the fingers descend, the gradient across the two-phase interface gradually decreases with time, but also diminishes earlier. This decreases the diffusion and therefore the dissolution rate starts to decrease. The peeling time seems to change with different height, as well as the angle. A twice-higher resolution shows a similar behaviour of the dissolution rate (Figure 16). Even

the angle seems to change. The higher the height, the lower the angle (Figure 15 & Figure 16).

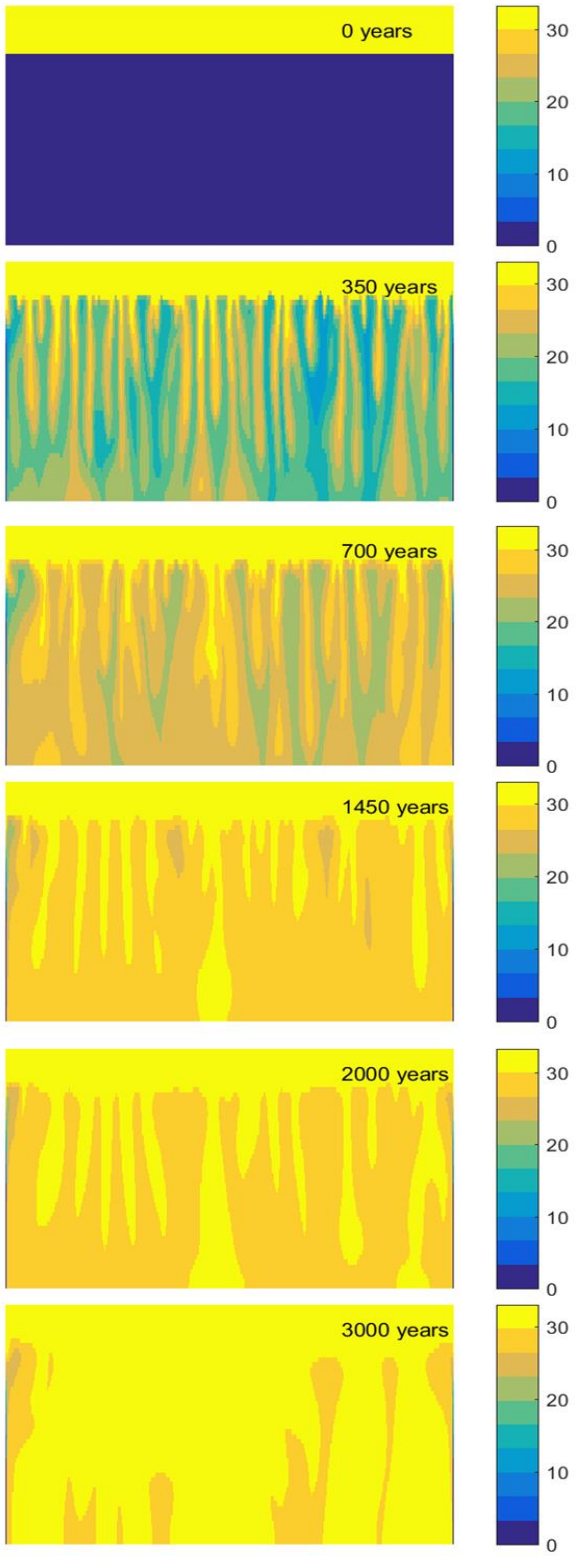

Figure 14: Dissolution of CO_2 (in kg) into brine caused by diffusion and convective mixing during 3000 years with no inclined aquifer.

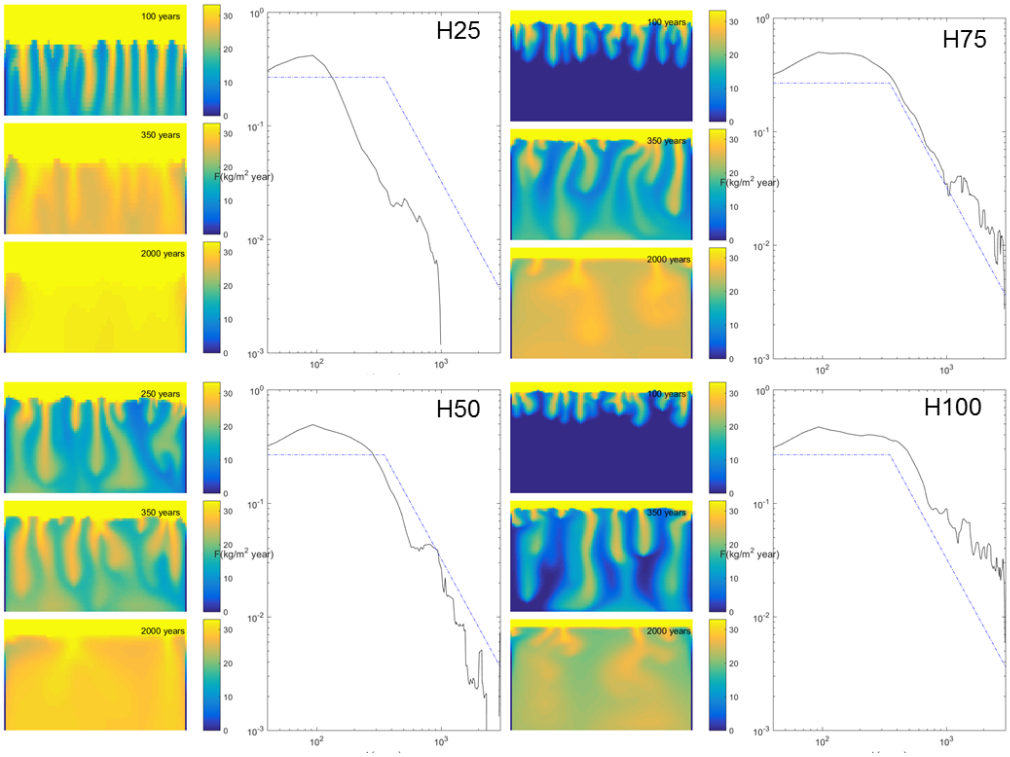

Figure 15: Dissolution of CO_2 (in kg/m^2 year) into single-phase brine caused by diffusion and convection mixing for the sensitivity of the size with a not inclined aquifer.

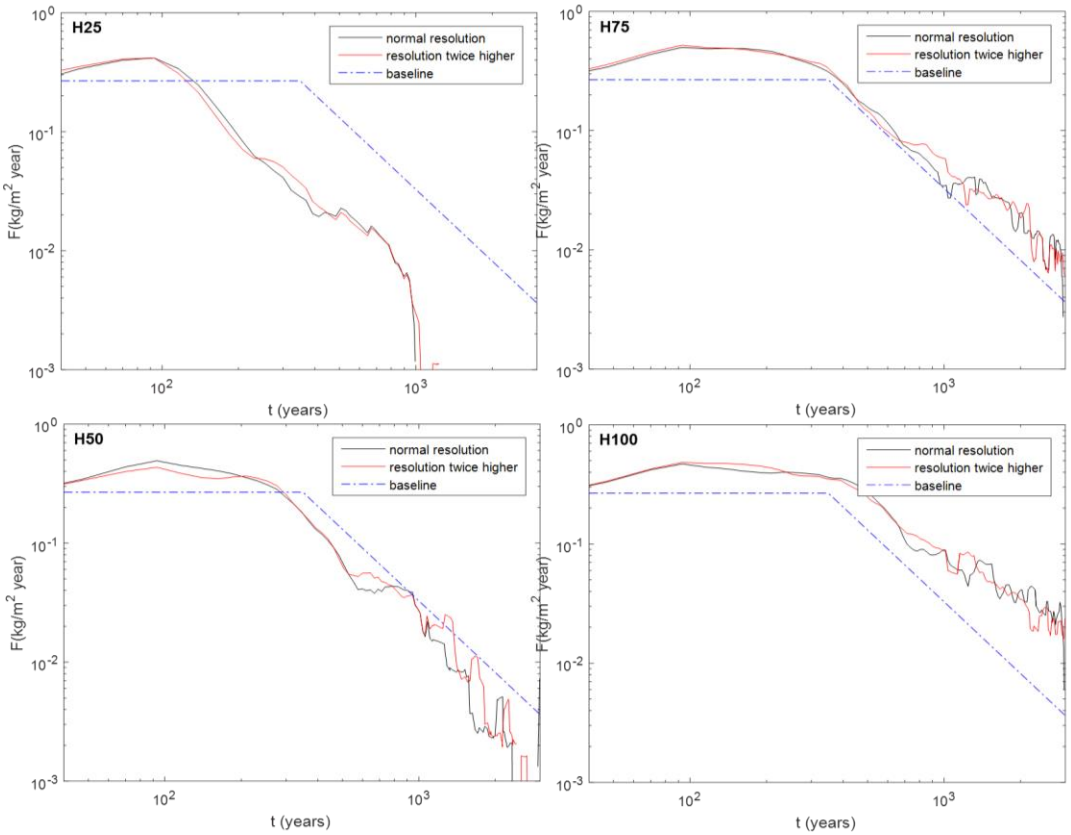

Figure 16: Comparison of dissolution of CO_2 (in kg/m^2 year) into single-phase brine for a non-inclined aquifer. The plots show heights of 25m, 50m, 75m and 100m, with a normal resolution and a doubled resolution.

6.3.1 Sloping aquifer

Fingers continue appearing until the domain fills up with CO_2. The dissolution rate reduces at late times. In a sloping aquifer the total dissolution rate can be effected (Maria T. Elenius, Nordbotten, & Kalisch, 2014) (Figure 17). The higher the inclination of the aquifer is, the slower the domain fills up (Table 6 and Figure 17). The dissolution rate until the t_{peel} is the highest for the smallest inclination, and the lowest for the biggest inclination (Table 6). The pressure difference in the upper layer is shown in Table 6. This pressure difference between these points will control the speed of the plume due to inclination. When the pressure difference in a layer is bigger, the distribution of the CO_2 mass is less over time Table 6 and Figure 17). The highest inclination (10°) need more time to be distributed, while the non-inclined model does not (Figure 17). This also indicates that there is less CO_2 mass distributed when the aquifer is inclined, but at the end of the 3000 years the mass distribution is almost similar for the different slopes (Figure 18). However, after t_{peel} the dissolution seems to behave similarly for the different slopes shown in Figure 17. In addition, the higher the inclination the later the decrease of dissolution rate starts because of the lower influence of low concentration and density gradients (Figure 17 & Figure 18). The stability results for a twice-higher resolution are compared with the normal resolution in Figure 20. Based on the results we can say that the rate until t_{peel} is lower for the higher inclination, there where the angle of reduction is sharper.

To quantify what is coming from physical inclination, and what from the speed of convection, a non-inclined model was used with the pressure gradient of a 10° inclined aquifer. This was also compared to a twice-higher resolution for a non-inclined aquifer. Figure 19 shows that the rate obtained from the higher resolution has a similar behaviour as the non-inclined aquifer. While the line obtained from the non-inclined aquifer and a pressure gradient of a 10° inclined aquifer shows a faster increase and a sharper angle for dissolution rate. From this result, it is clear that the inclination does have an impact on the behaviour of the speed of the plume, but not as much as the speed of convection in the model. The small difference shown in Figure 19 is due to the physical inclination.

Table 6: Dissolution rate before and after t_{peel} for different inclination numbers.

inclination °	until t_{peel} (kg/m^2 year)	after t_{peel} (kg/m^2 year)	Pressure first point upper layer (bar)	Pressure last point in same upper layer (bar)
0	**0.46**	**0.09**	**269.31**	**269.31**
1	0.37	0.09	267.96	265.22
2	0.32	0.08	266.62	261.13
3	0.28	0.09	265.27	257.03
5	0.23	0.11	262.58	248.86
7	0.16	0.13	259.89	240.69
10	**0.11**	**0.15**	**255.87**	**228.46**

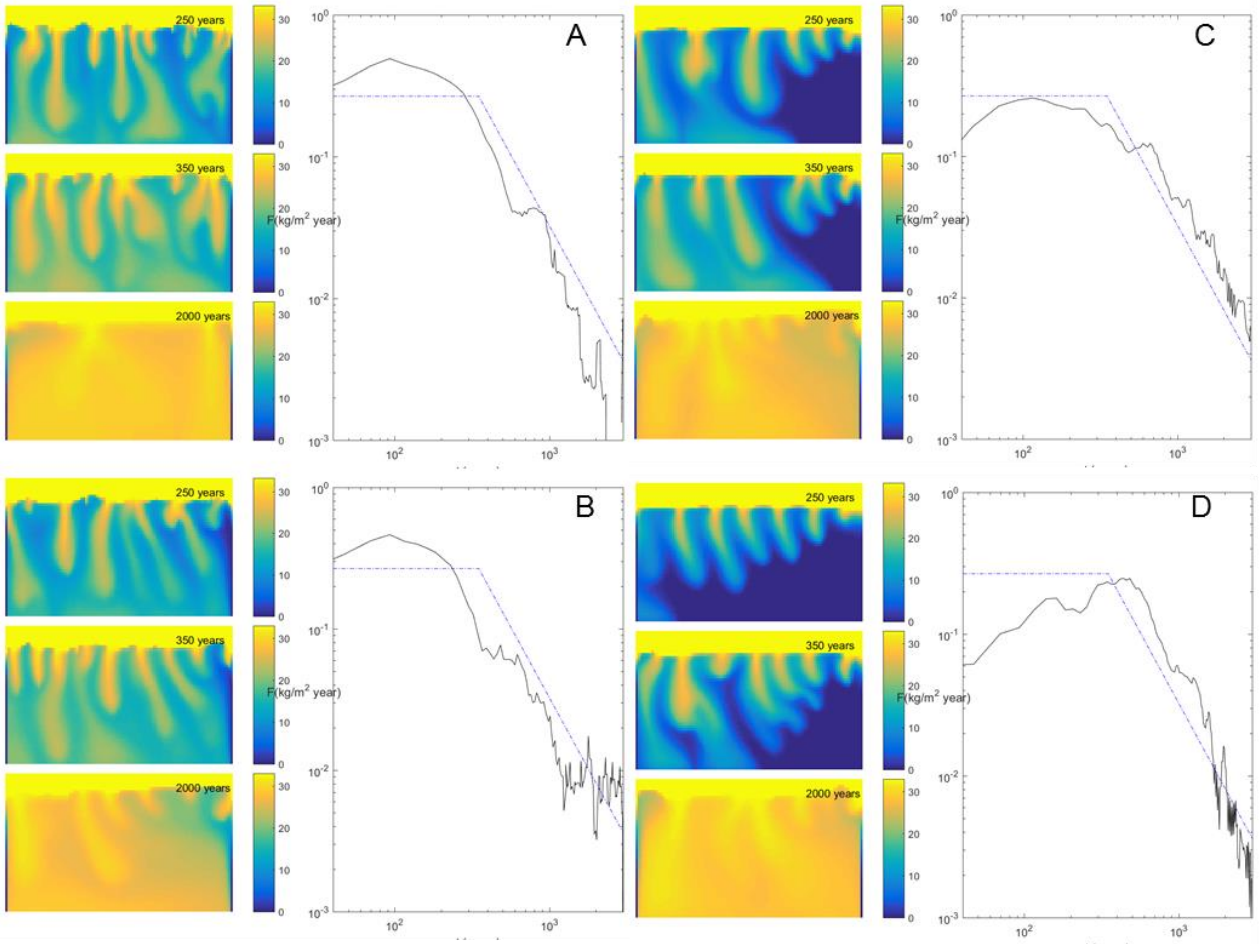

Figure 17: Dissolution of CO_2 (in kg) into single-phase brine caused by diffusion and convective mixing for the sensitivity of sloping. With A= no inclination, B= inclination 1°, C=inclination 5° and D=inclination 10°.

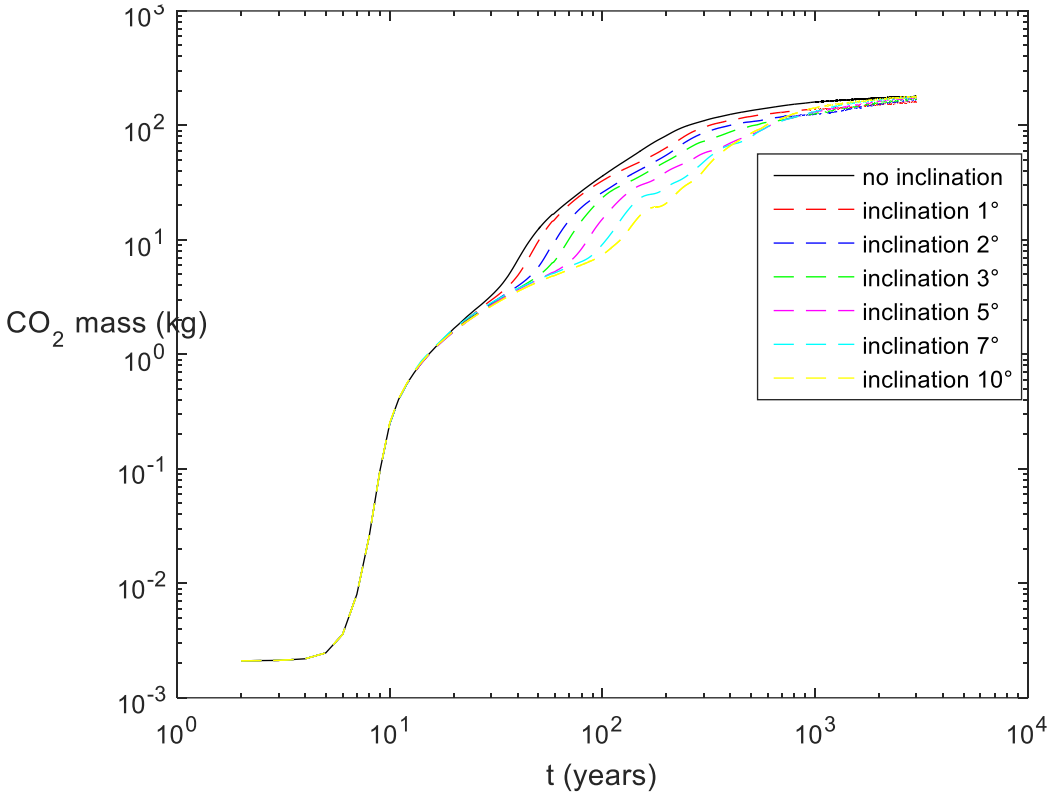

Figure 18: Distribution of CO2 mass over time in the reservoir with no slope, 1 °, 2°, 3°, 5°, 7° and 10°.

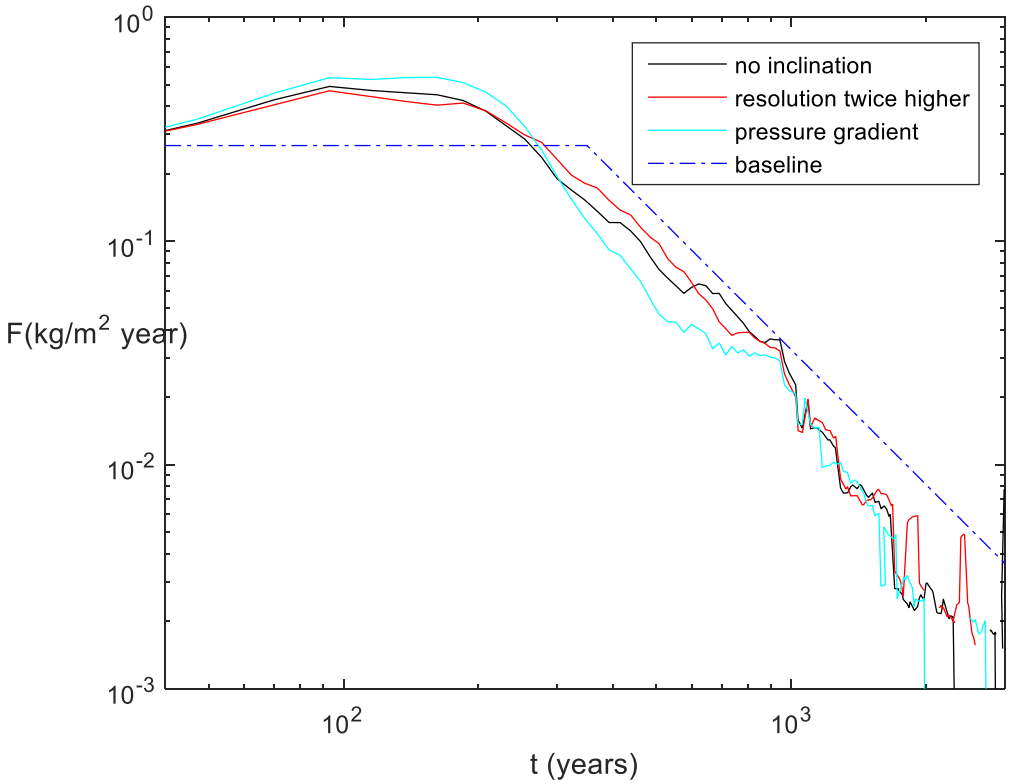

Figure 19: Dissolution rate over time for a non-inclined aquifer, a non-inclined aquifer with twice higher resolution and a non-inclined aquifer with a pressure gradient of 10°, compared to the baseline.

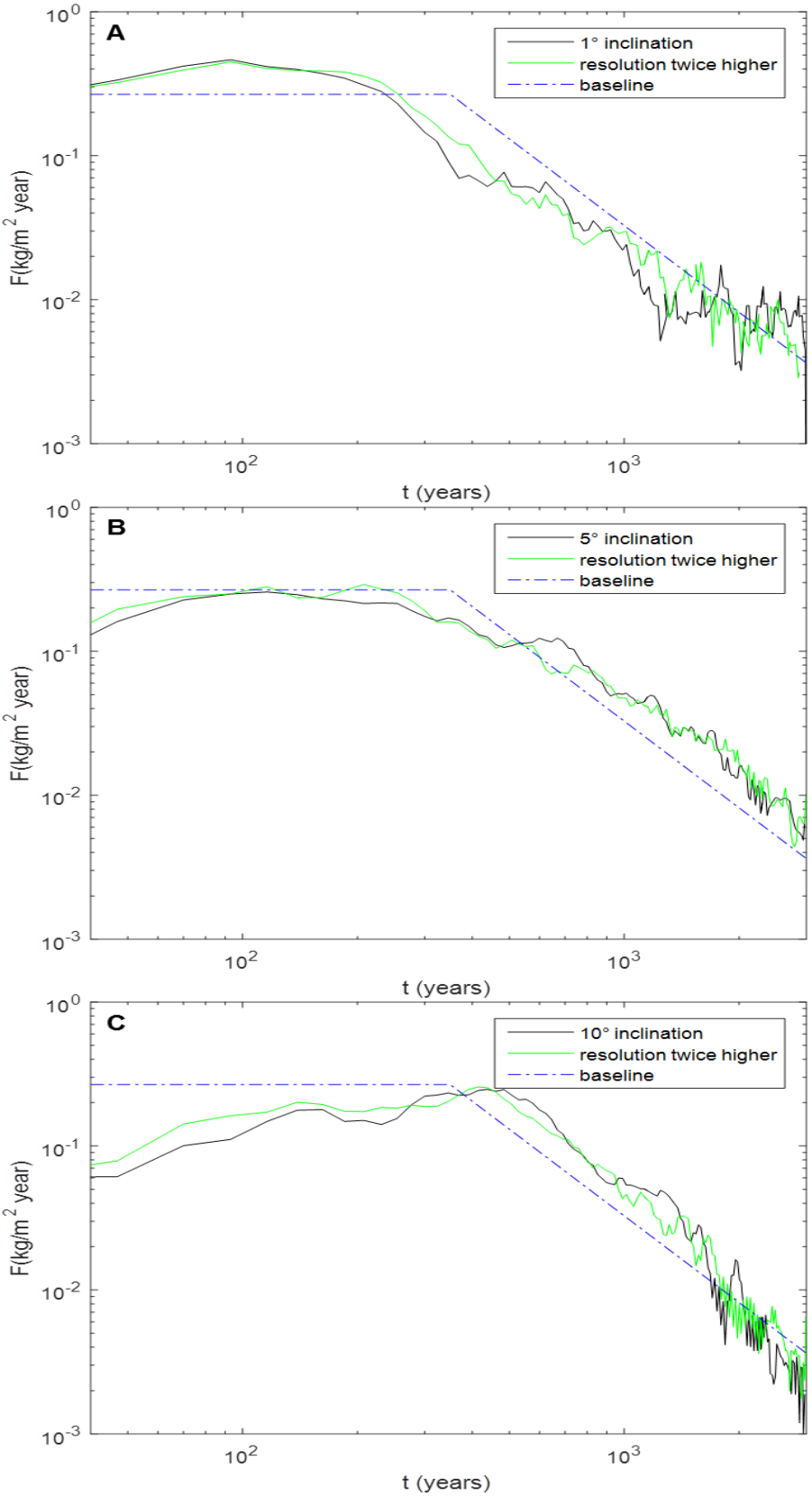

Figure 20: Comparison for dissolution rates with an inclined reservoir with twice-higher resolution. A: inclination 1°, B: inclination 5° and C: inclination 10°.

6.3.2 Relative permeability effect

The dissolution rate may vary in a domain with heterogeneous permeable layers (M. T. Elenius et al., 2015). Low-permeable layers influence the distribution of CO_2 strongly. This is because they block and delay the upward movement of the CO_2 (S. Gasda et al., 2011). A high-permeable reservoir shows smaller fingers compared to low-permeability reservoirs (Metz et al., 2005b). It was found by Elenius et al. (2015) that an increase in permeability values of the reservoir lead to an earlier switch from $t^{0.5}$ to the linear regime. In this type of reservoir solution trapping is effectively increased by convection, this might be the ascendant factor reducing the mobile CO_2 phase (M. T. Elenius et al., 2015). However, this finding is not confirmed for this thesis. The dissolution rate does not differ so much for the different relative permeability ranges. Relative permeability has very slight effect to fingering due to the changes in the transient zone. The fingering happened in 1-phase region which does not care about relative permeability.

6.3.3 Calculation sink term

To derive the dissolution rate from the small-scale models, three parameters were interested. These three parameters will later be used to be implemented as a sink term in ADGPRS. The positions of the three parameters are shown in Figure 21. The first number is an average of the dissolution rate from the beginning until the T_{peel} (number 2 in Figure 21). However, different inclinations of the small-scale model were taken into account. For the different inclinations the T_{peel} differs, also this was considered when making the calculations. Therefore, the T_{peel} is the second parameter and was calculated based on the second derivative. The second derivative measures how the dissolution rate is changing with respect to time:

$$second\ derivative\text{:}\ \frac{dF}{dt} = \frac{d^2x}{dt^2}$$

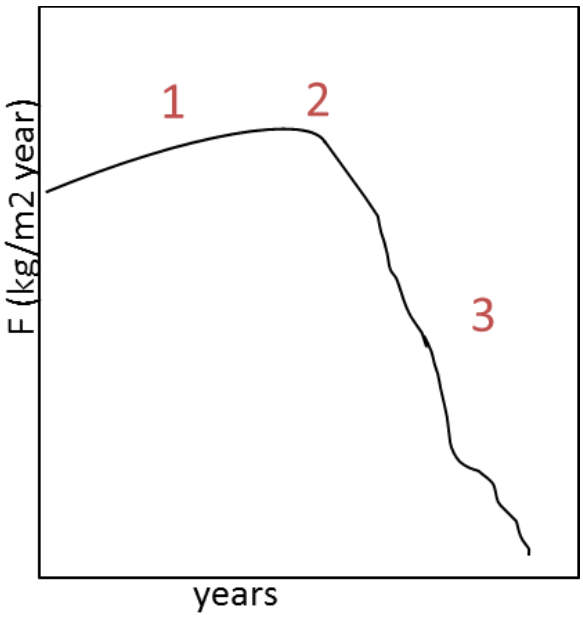

Figure 21: The 3 necessary parameters for sink term from the small-scale model.

The second derivative corresponds to the curvature of the graph. The graph of the function with a

positive second derivative bows downwards, while the graph of a function with a negative second derivative curves in the opposite way. To obtain the T_{peel} we looked up the highest positive second derivative of the numbers. For every inclination, the first 20 numbers included the time in years in which also the T_{peel} was reached. Therefor we looked up the highest positive second derivative of these 20 numbers. The highest second derivative outcome is the point, which is called the T_{peel} (shown in Figure 21 with the number 2). We then took the average of the rate until the biggest second derivative outcome (this is shown with the number 1 in Figure 21). From the T_{peel} the dissolution rate starts to decrease. Until the CO_2 reaches the bottom of the reservoir. The third parameter was chosen based on the biggest change in the rate after the T_{peel}. The behaviour before this third point was more continuing compared to the other points. The three parameters are different for every inclined model. The models are based on a 400-meter length, a 50-meter height reservoir, and an inclination condition of 0°-9°. The three parameters shown in Figure 21 for all the different inclinations were obtained. An example of the model with inclination 2° is shown in Figure 22. With the fitting line method, the first and second parameters were extracted. The linear green line until the red circle represents the first parameter, which is the initial rate (y1 in the figure); the second number is the rate at time t_{peel}, which is subtracted from the position of the red circle. The red circle is the interaction point between the two (green) fitting lines. The third parameter is based on the initial rate divided by two.

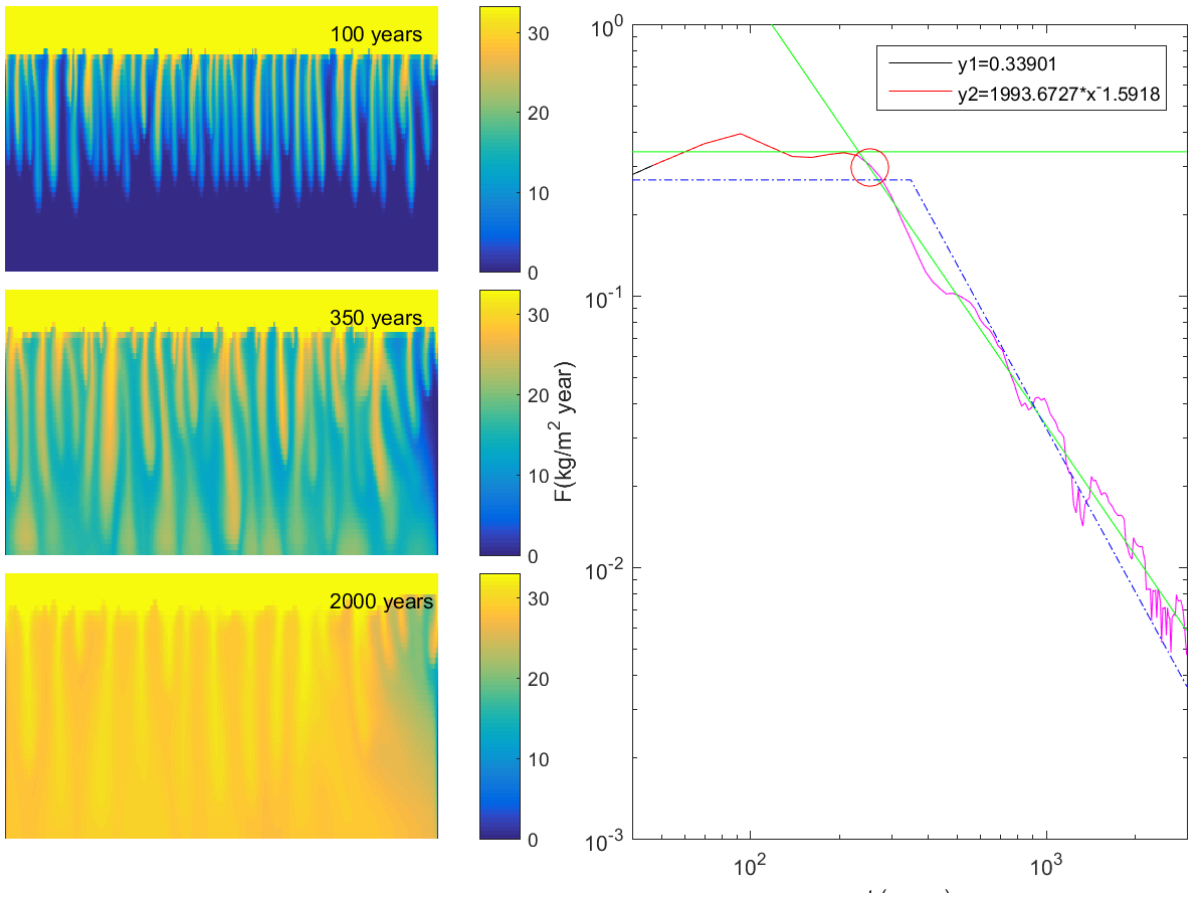

Figure 22: The fitting lines for inclination 2.

The parameters for the inclination condition of 0°-9° were collected in the same manner as for Figure 22

and are shown in Table 7. These parameters will be necessary later for the large-scale model.

The three parameters per inclination condition were then plotted against one another (Figure 23). The highest inclination takes the longest time until it reaches the time where the dissolution rate starts to decrease (t_{peel}). The higher the inclination, the more time it takes until the reservoir is filled with CO_2. From inclination 7-9° the differences are small, and the changes are almost negligible. The lower the inclination is the higher the initial dissolution rate is. All the fingers can equally dissolute in the reservoir. The area under the graph for the different inclinations is the same, since we are dealing with the same reservoir.

Table 7: For length 400 the inclination and the three parameters per inclination model.

L400			
Inclination	Initial rate (kg/m² year)	Tpeel (year)	Initial rate / 2 (year)
0	0.376036	254	338
1	0.353232	208	313
2	0.339012	254	361
3	0.298301	300	445
4	0.274675	323	478
5	0.263901	369	518
6	0.228893	369	518
7	0.228833	438	613
8	0.217285	461	642
9	0.223986	484	648

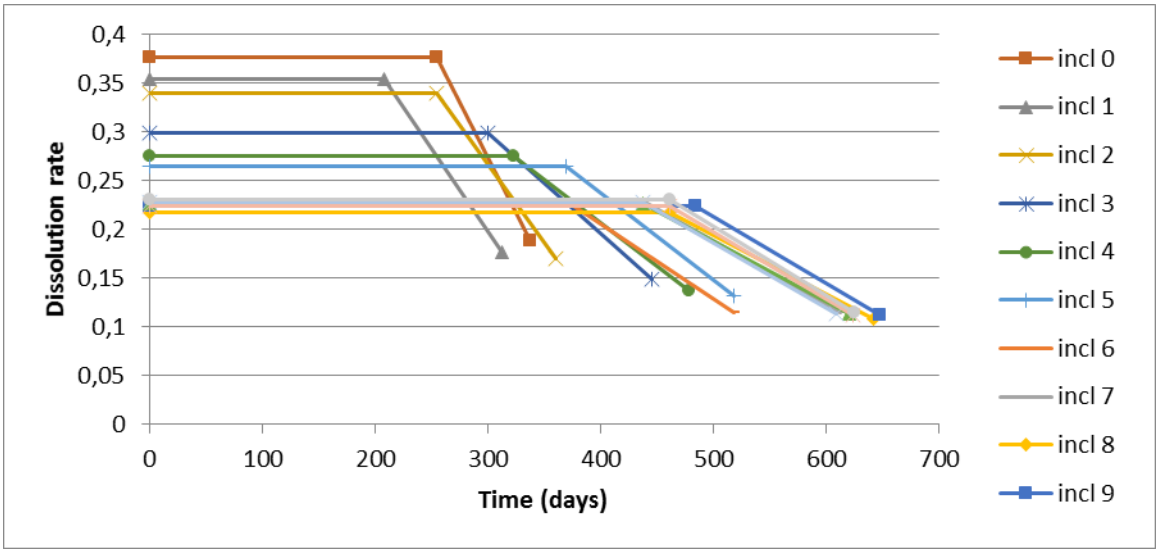

Figure 23: Dissolution rate vs. time for small-scale model inclinations between 0°-9°.

6.3.4 Implementation of sink term in small-scale model

The parameters obtained in Table 7 are implemented as a sink term in the small-scale models. This to confirm that the method we are using does work. First, we plotted the model without density difference between CO_2 and brine, therefor molecular diffusion cannot take place and instabilities will not translate into fingering. As expected, there is no dissolution nor diffusion, nor a rate observed (Figure 24). In this model, we then implement the sink term to see weather this provides an expected rate (Figure 25).

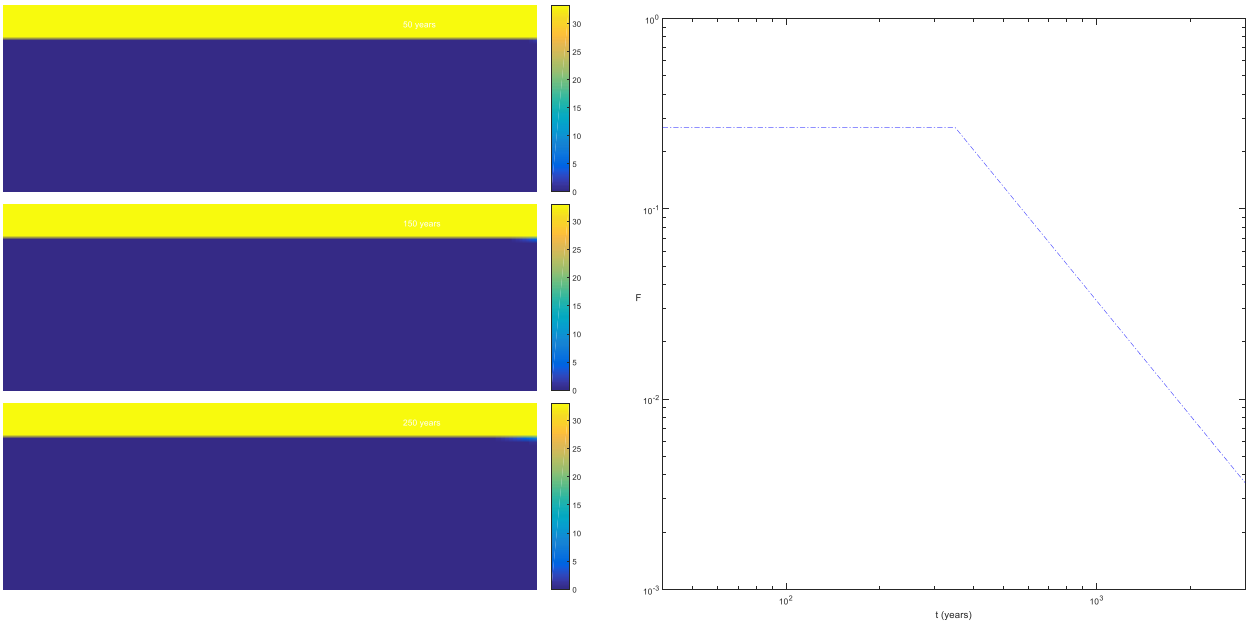

Figure 24: without diffusion but no density difference for 2-degree inclination.

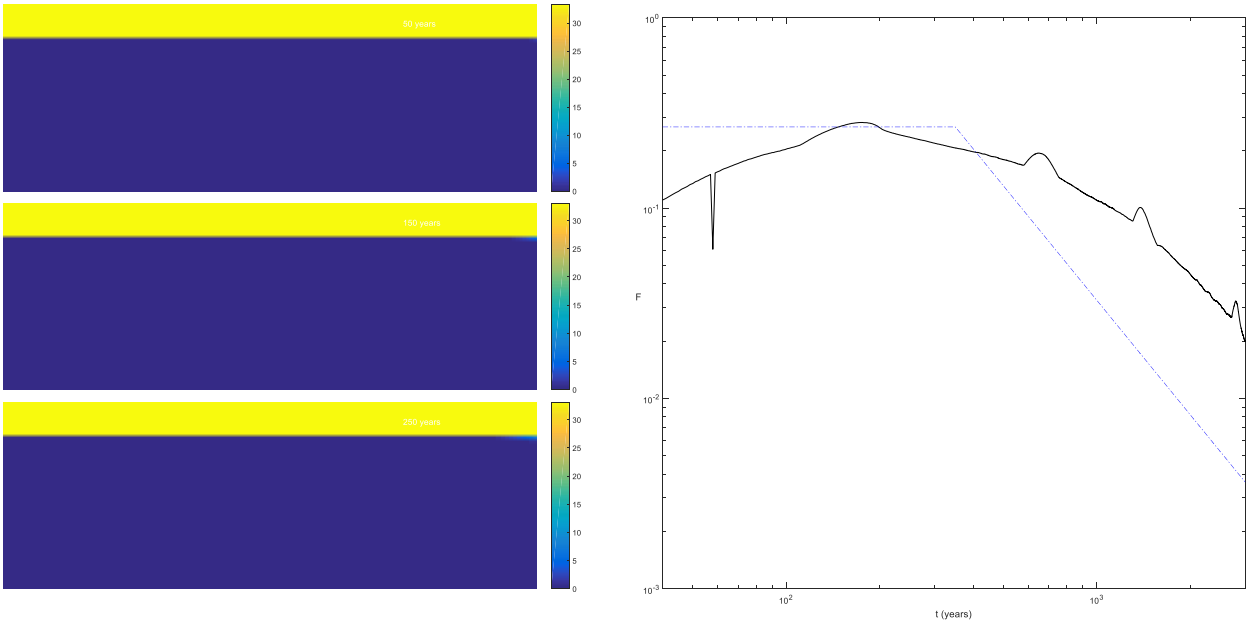

Figure 25: without diffusion but with parameters but no density difference for 2-degree inclination.

6

Results & Discussion

Large-scale

6.4 Upscaling

To get an inside in the safety and the effectiveness of CO_2 storage in formations, it is necessary to simulate the convective process accurately. Heterogeneity should be considered for the miscible viscous fingering instabilities. However, for this thesis, the absolute permeability is assumed to be homogeneous and isotropic, and the porosity and viscosities are constant. These assumptions are made to reduce the complexity of the model and only focus on the effect of dissolution trapping. It is very time consuming to simulate the density fingering over long times at the field scale to predict the movement of CO_2 underground (M. T. Elenius et al., 2015). To upscale simulation results from the small-scale to the large-scale, a two-scale discretization of the grid was used. In the first scale, the dissolution rate, obtained at small-scale model was applied when for the first (finer) scale, the convective propagation of CO_2 plume was applied. This approach was compared with the direct fine-scale simulation results by the end of this chapter.

6.5 Large-scale model problem

For the large-scale problem, the plume migration was first observed for an aquifer with a slope of 0°, 1°, 2°, 4° and 8° (Figure 26). The plume migration for the different slopes was modelled. The aqueous phase plays different roles affecting the evolution of the CO_2 plume. Firstly, it serves as a medium for pressure transmission, secondly it occupies pore space. This pore space must be forsaken to make it possible for the CO_2 plume to advance. Thirdly, it can serve as a sink since it can dissolve CO_2. Fourthly it is a transport medium for dissolving CO_2 by diffusive and advection processes. The CO_2 plume will displace the water outwards when it advances. Beyond the gas, front water flow is in downward and outward direction, away from the plume. In the plume, there is also a small water flow downward (Riaz et al., 2006) (Figure 26). Dissolution occurs via diffusion without convective enhancement in regions far from the edge of the source. This process causes a diffuse layer of CO_2 rich fluid right under the saturated CO_2 at the top boundary. Convection begins immediately since the smallest amount of diffusion leads to a lateral concentration gradient there, which drives vertical flow. This breeding of the finger disturbs a bordering region of the CO_2 rich boundary layer, which destabilizes the layer and thereby creates a contiguous finger. This process increases the fingerings along the source. When there is a physical or numerical perturbation, the entire boundary layer destabilizes and therefor fingering stops (Pruess & Nordbotten, 2011). The example is shown in Figure 26.

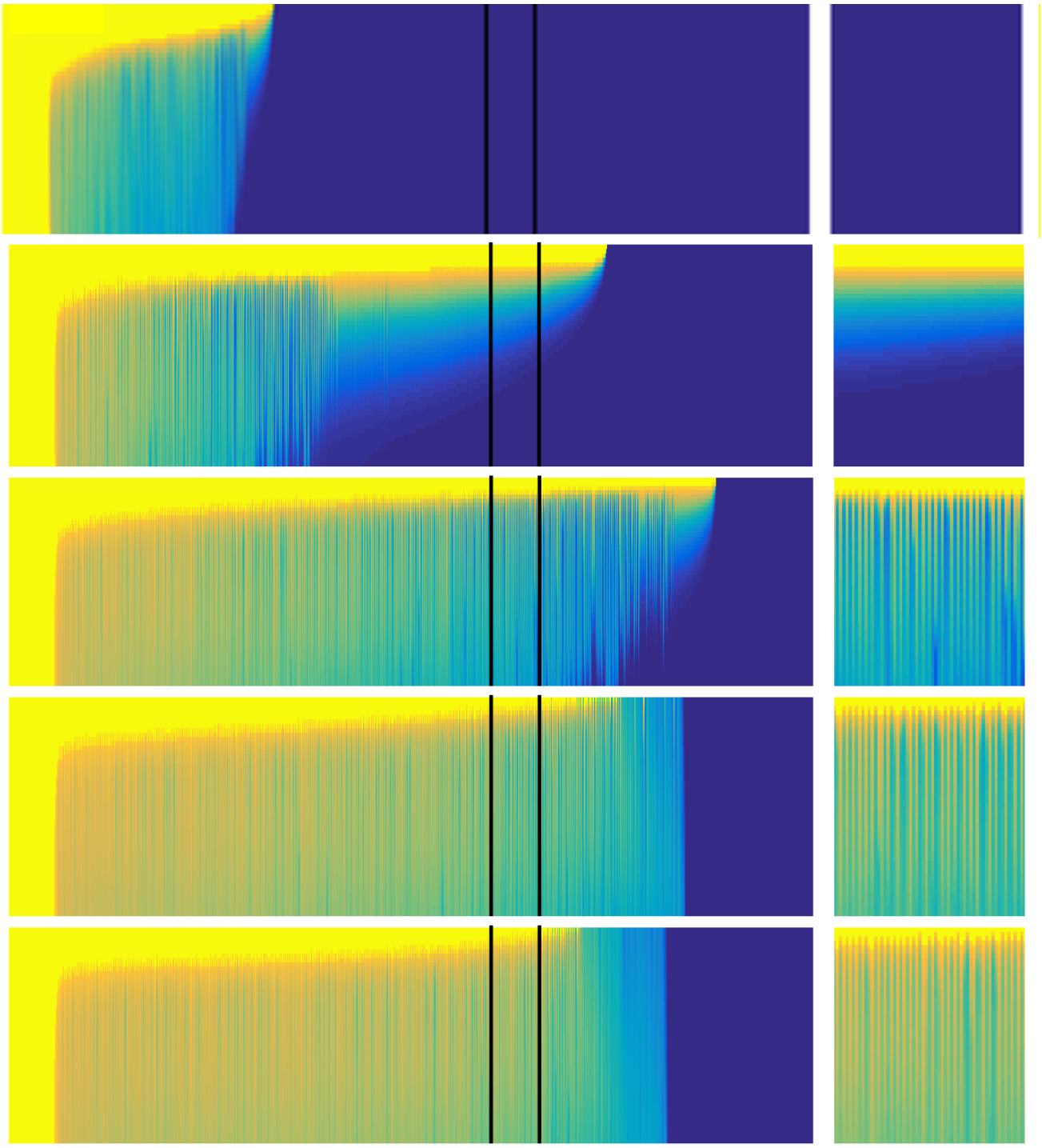

Figure 26: Plume migration for a large-scale model with, from top to bottom, 0°, 1°, 2°, 4° and 8°.

Keeping the time constant for the different slopes, shows that at a certain time, the fingers are more dense and narrower for the higher degree of slope than the small once. From the dissolution rate plot (Figure 27) it is observable that the rate stays higher after the maximum dissolution rate is reached for the highest inclined domain. This is comparable with the small-scale results (Figure 28) in which also a higher dissolution rate is shown after the t_{peel} was reached when the inclination is.

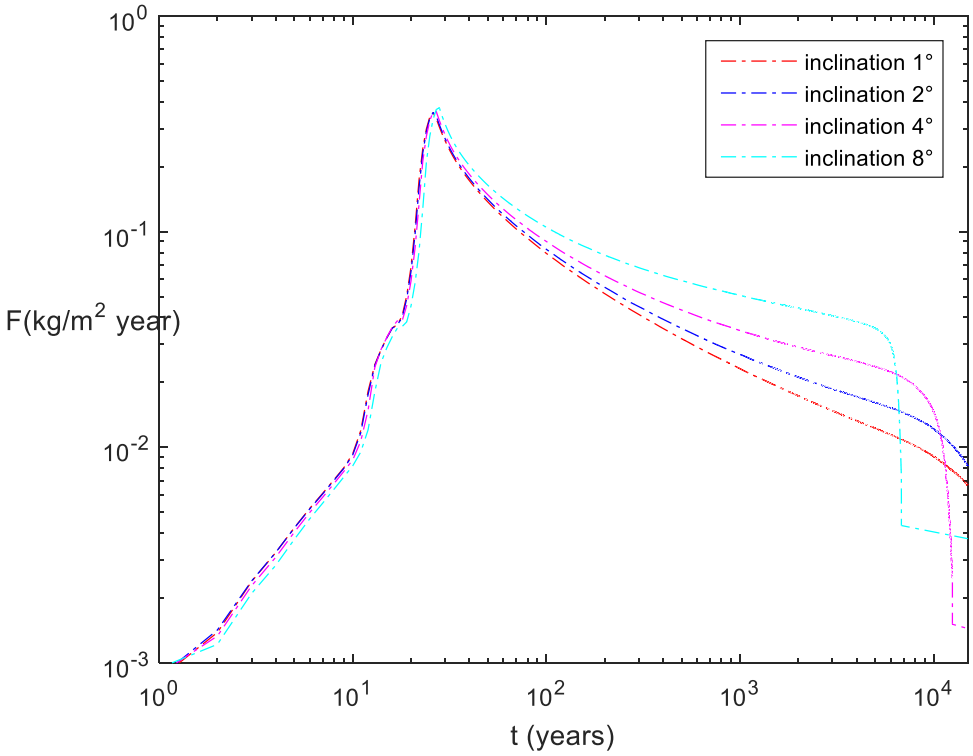

Figure 27: dissolution rate for large-scale model.

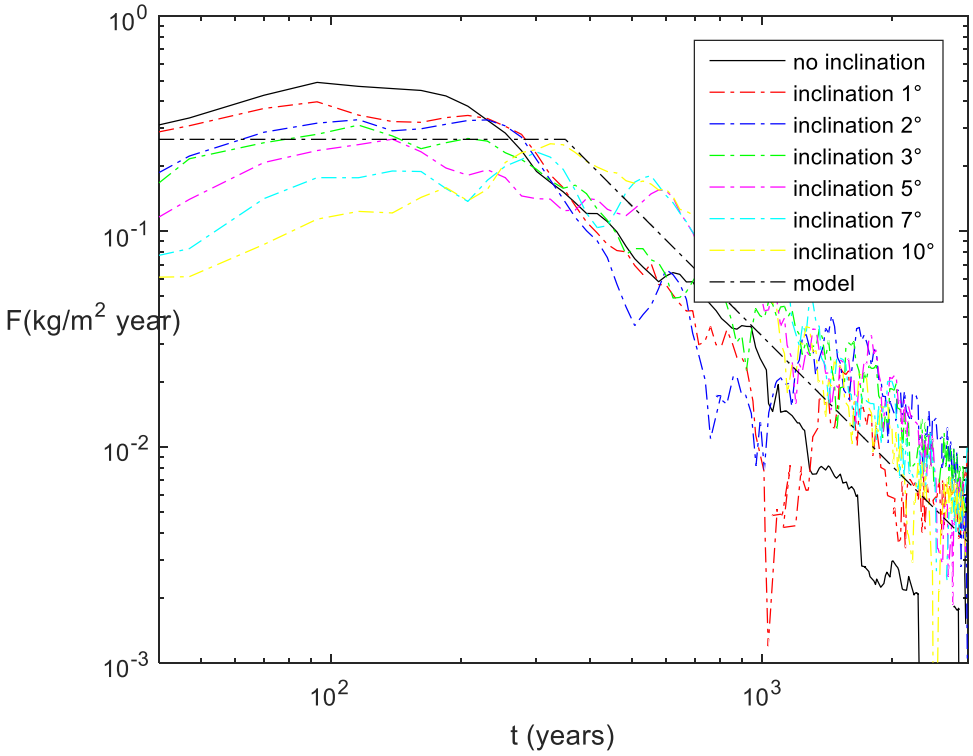

Figure 28: dissolution rate for small-scale model.

In a more realistic geological system like the Johansen formation, the rates of CO_2 migration will be effected by heterogeneity and structural complexity. In such a system, a low or high permeability can

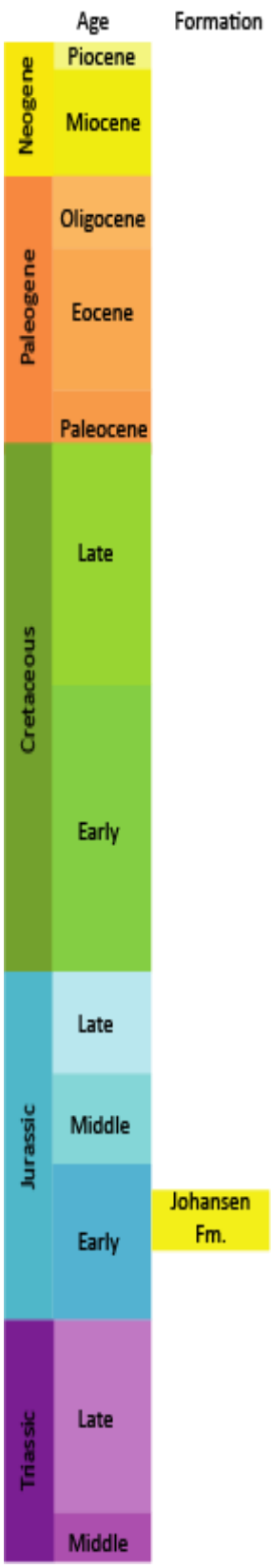

Figure 29: Age of the Johansen formation.

both show a relatively slow migration rate, because of the causing features named earlier (heterogeneity and structural complexity). From the large-scale model in Figure 26 it is clear that after a while, the extension of the plume from the injection point stops. This is because of the combination of convection-enhanced dissolution and residual trapping together with the slow migration rate, which leads to complete immobilization after a thousand years. ''It is therefore important to consider the long-term immobilization of CO_2 as largely dependent on the properties of the system of interest'' (Szulczewski et al., 2013). A slice from the more realistic geological system of the Johansen formation (Figure 31) was used to observe the effect of dissolution rate according to the height and inclination of each block in this formation.

6.5.1 Johansen Formation

The Johansen formation is a candidate site for large-scale CO_2 storage offshore the south-west coast of Norway. The Johansen formation is from the lower-middle Jurassic (Figure 29). It is a deep saline aquifer, which is located approximately 600 m below the sandstone layers of the Troll-field. The Troll field is the world's tenth biggest offshore gas project. It accounts for approximately 40% of the total gas reserves in Norway. The Johansen formation has a large volume, it suits pressure regimes at the large depths, and it has close well access from the Troll-field, therefor this formation is a promising formation for CO_2 storage. The formation contains shale and sandstone (Eigenstad et al., 2009). An overview of the geological model of this formation is shown in Figure 30. Only one slice out of the whole formation was used for our research question. A slice with the biggest inclination differences was considered, in which the parameters obtained from the small-scale were later implemented. The used slice and the depth differences are shown in Figure 31.

.

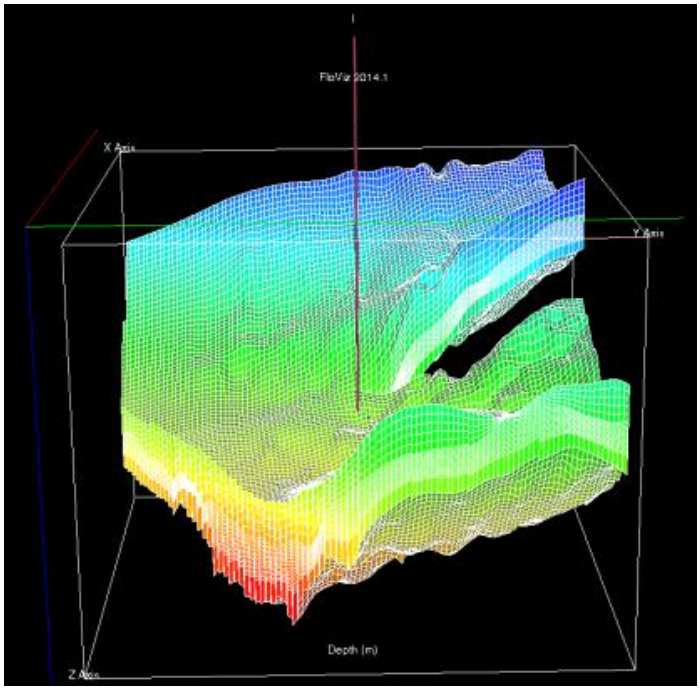

Figure 30: Overview of the geological model of area in depths of the Johansen formation.

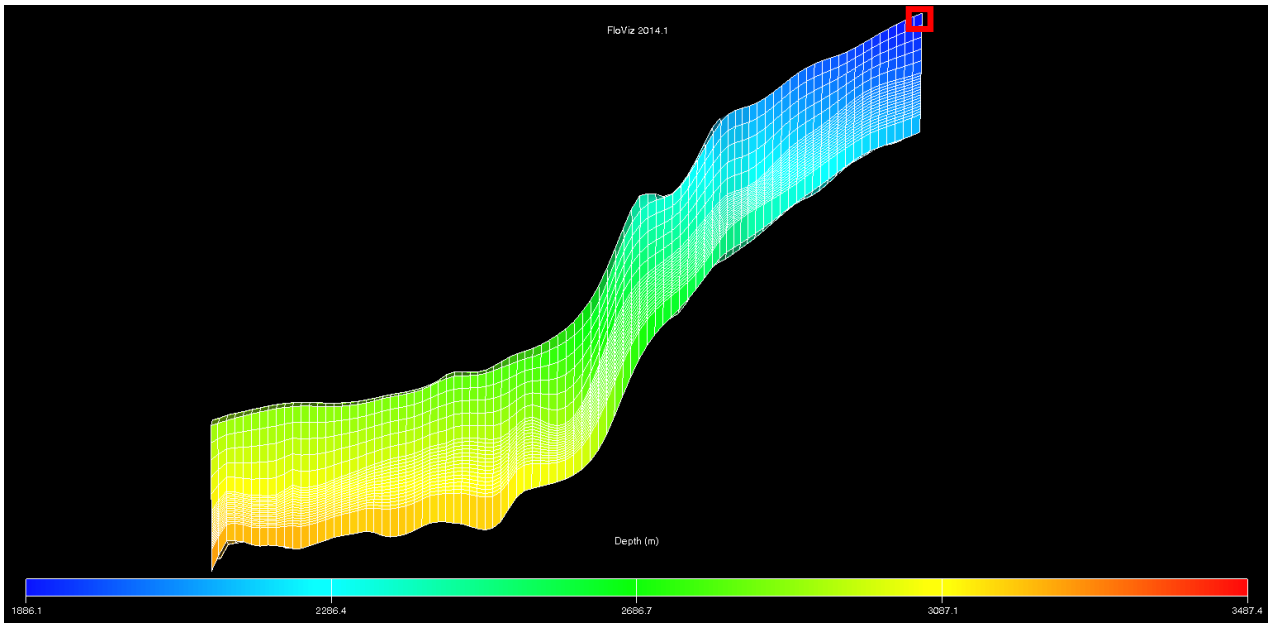

Figure 31: A slide of the geological model of the Johansen formation that is being investigated for CO_2 storage .The red box represents one block of the upper layer. The depth for every block can be extracted. The dimensions of the displayed slide are dx:dy:dz 1:1:25.

First, the depth of the top boundary of the layer in Figure 31 was obtained using Petrel Floviz Eclipse simulation. The depth of every single block on the top boundary layer was used to get the most accurate results. There were 88 regions from where the depth could be obtained using Petrel Floviz Eclipse simulation. The total length of the slice was assumed to be 20.000 meter. The depths and the total length was then used for the discretization of the coarse and fine scale model. The inclination of every region in the slice of the Johansen formation was based on the first and last point of Petrel depths and the total length of the reservoir. The regions were interpolated over the whole reservoir. For the calculation of

the inclination angle anywhere in the reservoir, the depths for the blocks and the neighbouring block was used. The equation used to calculate the inclination angle is shown in equation (18).

$$inclination\ angle = \cos\ (depth_{block}(i) - depth_{block}(i+1)) \quad (18)$$

The first region (from left to right) is the CO_2 injection region; the CO_2 migration will take place on the right side of the injection area (Figure 7). The grid block sizes of dx=1, dx=2, dx=4, dx=20, dx=100, dx=200 and dx=400 were simulated to make comparison of plume migration and tip position possible between the different resolutions. 'dx' represents the size of the grid blocks in x-direction in meters. The depths of the used slice are between 2938.3 meter and 1886.1 meter.

6.5.1.1 Coarse scale model

For the course scale model, a grid size in the x-direction (dx) of at least 20 meters was used. The total length of the reservoir (20.000m) was divided over the total grid blocks. The depths obtained from petrel were extrapolated to the real reservoir length of 20.000 meters (Figure 32). These depths were then interpolated, which results in a continuous line (Figure 34). In Figure 32, a discrete version of the reservoir is shown.

The interpolation was made based on the total length of 20.000 m and the 88 depths we have extracted from Petrel Floviz Eclipse: 20.000/88= 227m per depth difference. Then the depth difference was calculated and divided over the 227 meters. This depth was then added to the previous depth (Figure 33). The interpolated version of the reservoir depths is shown in Figure 34. Figure 35 shows the CO_2 plume movement in the slice with full physics of dx=20 for the Johansen slice with interpolated depth in the reservoir.

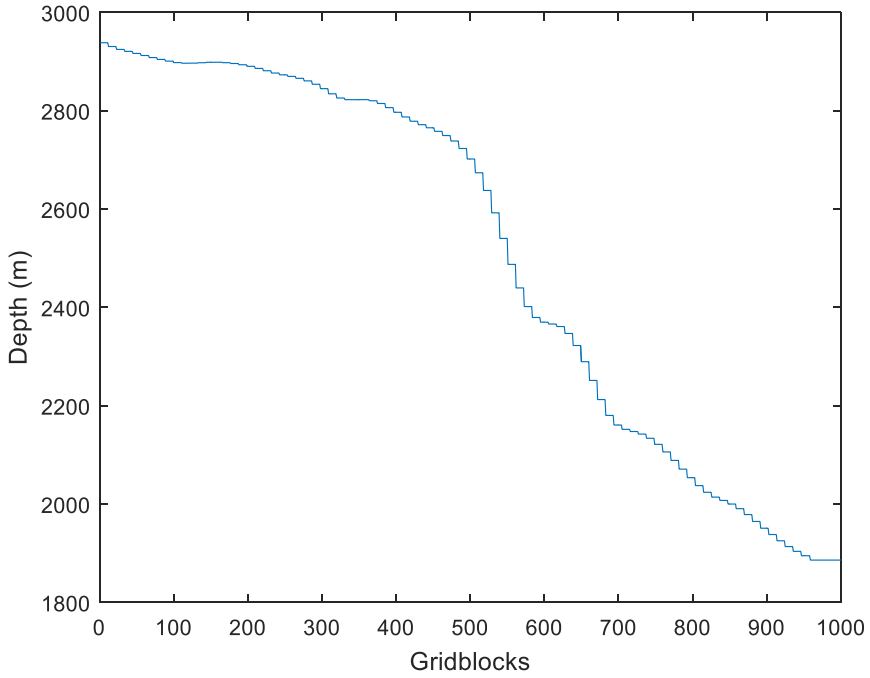

Figure 32: depths for the total length of the reservoir of 20.000 m with a dx=20m calculated from the real depths from petrel, without interpolation.

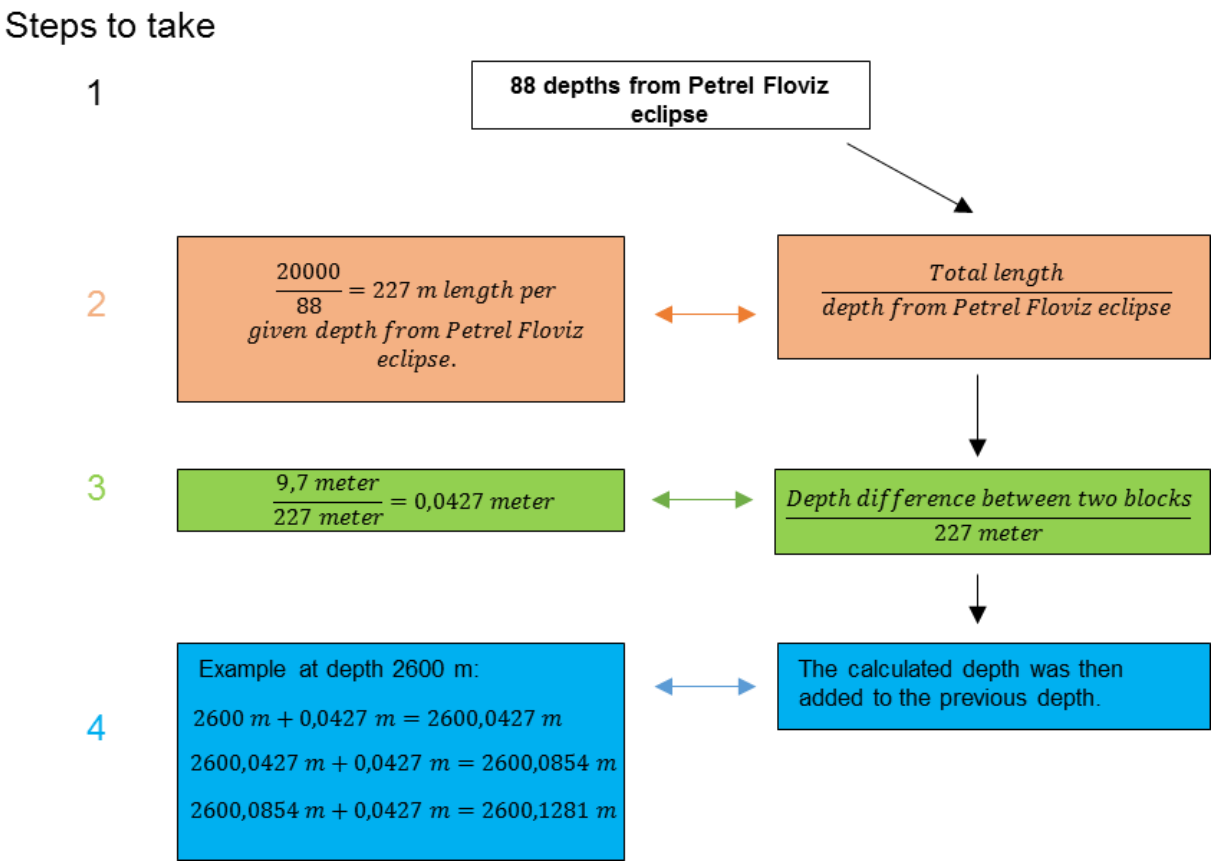

Figure 33: Steps to take from no interpolation of depth (figure 33) to interpolation of depth (figure 35).

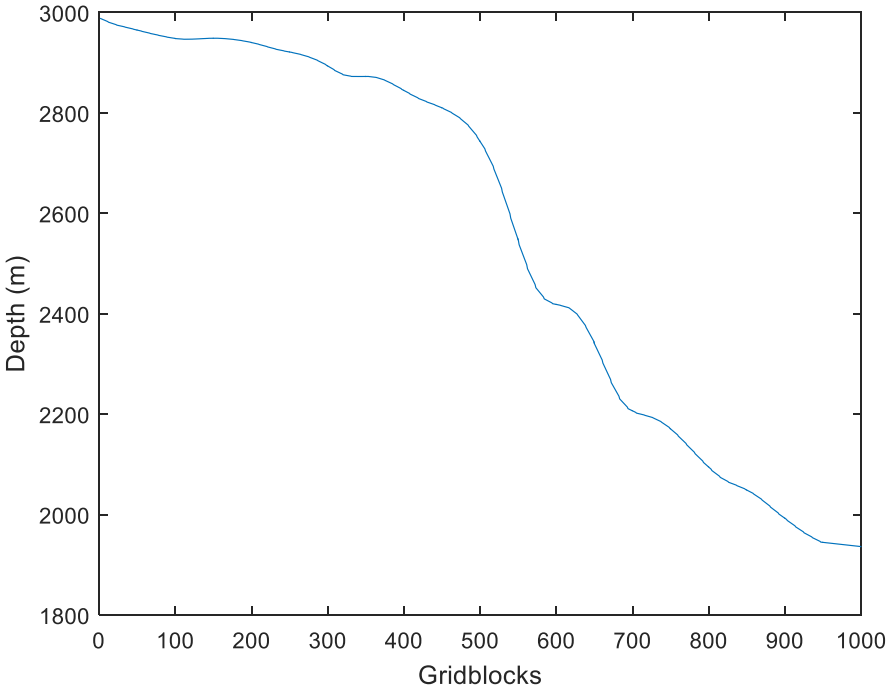

Figure 34: Interpolated depths for grid blocks with dx=20m and length of reservoir of 20.000

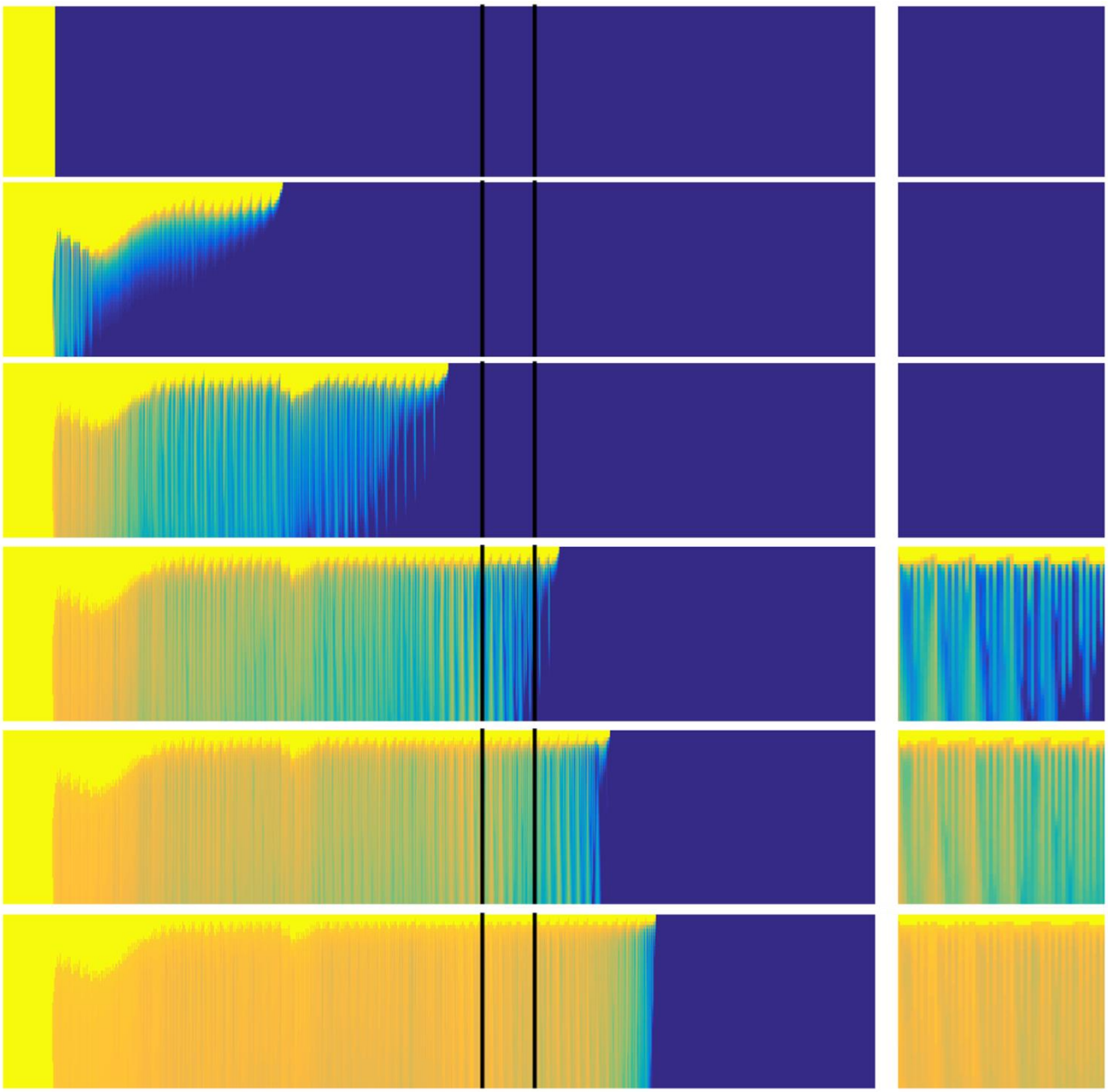

Figure 35: CO_2 plume movement in the slice with full physics dx=20 for the Johansen slice.

6.5.1.2 Fine scale model

The fine scale model is used as reference data for the coarse scale model, but also later for the proxy model. The proxy model is the large-scale model without diffusion or dissolution, in which the sink term will be added. Since in this model the gridsize is twenty times smaller (dx=1), the area of the gridblocks is also smaller. The fingering in each block will be closer to one another. This results in a more accurate migration of the plume.

6.6 Case study

Firstly, we studied the detailed behaviour of finger propagation and the associated dissolution rate in small-scales. Than we proceeded with the dissolution rate in larger scale. Here we present the dissolution rate for full physics for the coarse models (Figure 36) and the fine models (Figure 37).
Clearly, the fingers of a fine-scale simulation (dx1) propagate more and therefor the dissolution rate in the presence of a finer grid is higher than it does for the coarser grid. However, a grid size of 20m x 1m and finer does not show a significant difference in dissolution rate (Figure 37). While the coarse grid size shows a big difference in dissolution rate between 400m x 1m and 100m x 1m (Figure 37). The simulation with 20m x 1m grid produces the highest concentration in the fingers, and therefore appears to be the most efficient option for representing the dissolution trapping (Figure 37 and Figure 37). Convective mixing, which is associated with the fingers, is enhancing the dissolution rate. The lower the grid block size the more accurate the results are, and therefore the higher the dissolution rate can reach. An overview of the numbers of blocks, the running time and the CFL are shown for dx400, dx200, dx100, dx50, dx8, dx4, dx2 and dx1 in Table 8. The finer the model, the higher the runtime, but also the higher the maxCFL averaged by time steps (Table 8).

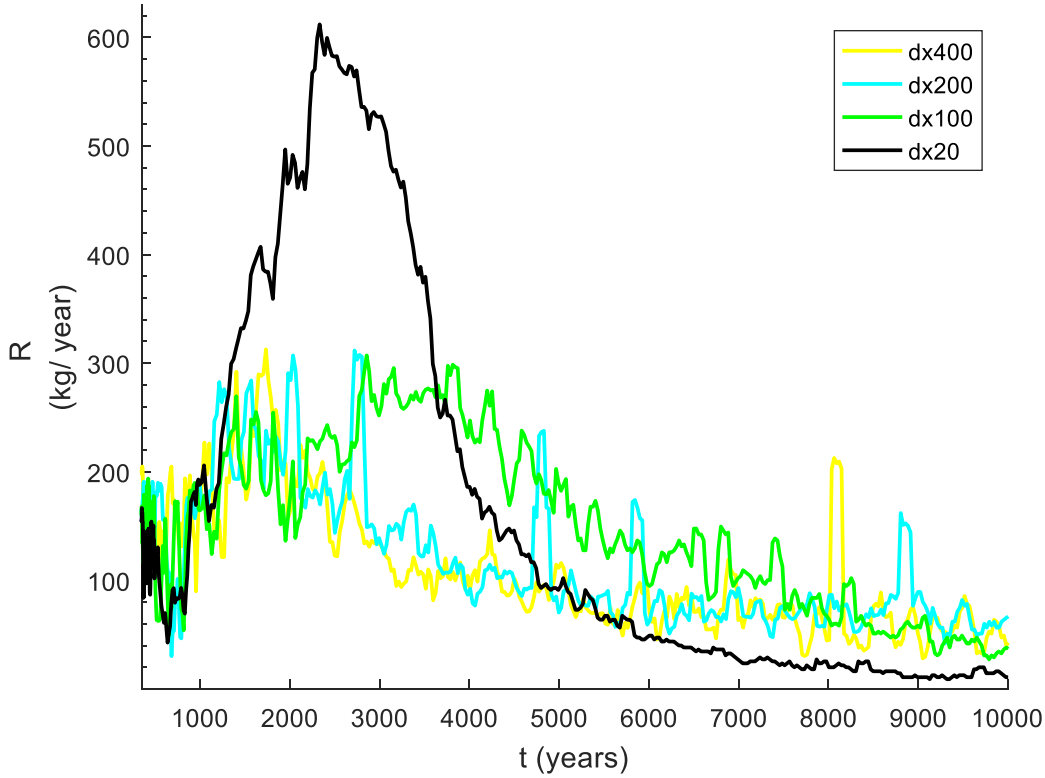

Figure 36: Dissolution rate into single-phase brine (kg/year) for the coarse scale models dx400, dx200, dx100 compared to dx20.

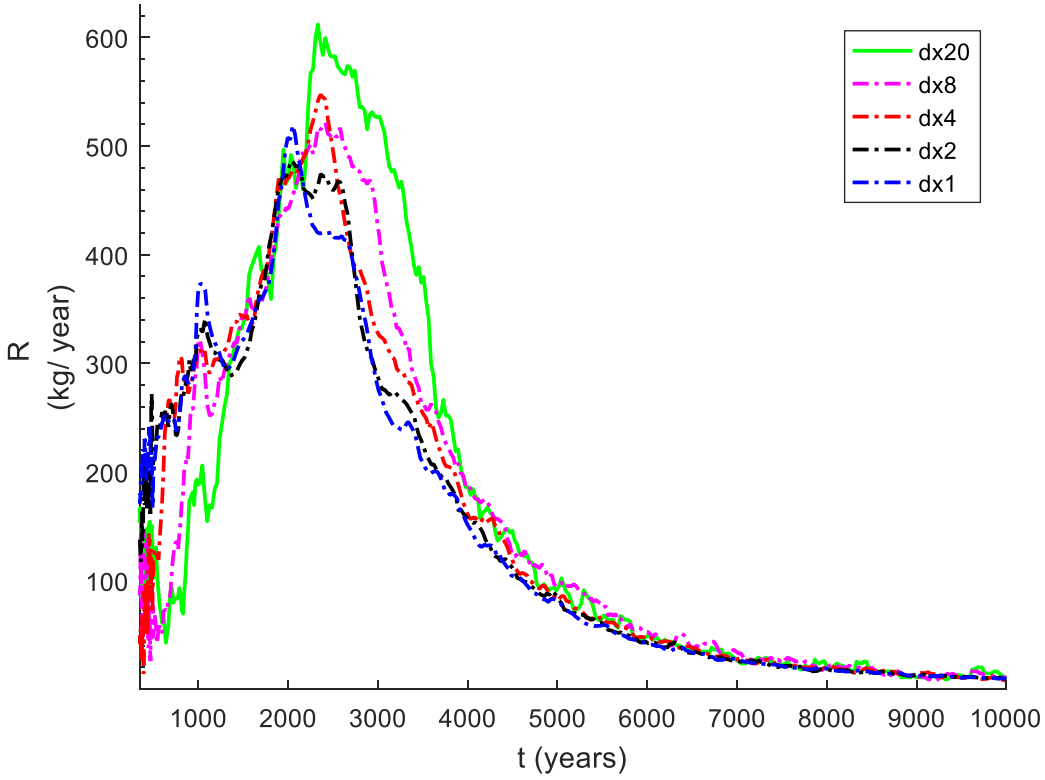

Figure 37: Dissolution rate into single-phase brine (kg/year) for the fine scale models dx8, dx4, dx2 and dx1 compared to dx20.

Table 8: Overview of the numbers of blocks, the running time and the CFL are shown for dx400, dx200, dx100, dx50, dx20, dx8, dx4, dx2 and dx1 for different models.

Model	dx	dz	L (in meter)	H (in meter)	run time in hours	number of blocks	MaxCFL averaged by time steps
dx400	400	1	20000	50	3.5	2500	0.013
dx200	200	1	20000	50	21.7	5000	0.019
dx100	100	1	20000	50	15.1	10000	0.03
dx50	50	1	20000	50	69.1	20000	0.05
dx20	20	1	20000	50	93.57	50000	0.004
dx8	8	1	20000	50	291.0	125000	0.157
dx4	4	1	20000	50	273.7	250000	0.357
dx2	2	1	20000	50	778.6	500000	0.66
dx1	1	1	20000	50	1742.4	1000000	1.232

The saturation profile, plume migration and dissolution rate were then plotted for the Johansen formation slice with a grid block size of dx20 (Figure 38). The first plot shows the gas saturation, the second shows the CO_2 composition and the third shows the dissolution rate. The three plots are shown three times for 2000, 6000 and 12000 years. The plot shows that the CO_2-rich fluid floods on top of the water-rich fluid, due to a difference in density. At the interface of the two fluids, dissolution takes place. The plume is migrating up-dip near the top of the permeable layer. It then keeps migrating under the sloping cap rock. The migration of the plume in the initial period is rapid because of the strong driving force. When CO_2 goes up, the water goes down, this because of the buoyancy forces. The instability of the CO_2–rich brine on top of the aquifer layer initiate a convection current. Brine without CO_2 is moving up to the interface while the CO_2-rich brine moves downwards. We see this behavioural already after 2000 years. The pure CO_2 is on top, which enhances dissolution which in turn shows will show fingering.

The fingering increases between 2000 to 6000 years. In addition, the dissolution rate increases. This accelerates the dissolution process, and hence the mass transfer rate. The speed of the plume decreases when dissolution is considered, until it reaches a constant value after the transition period. Subsequent advancement continues then with a constant speed. The plume is thinning out the further it migrates. Together with the out thinning plume, the mass flow of the CO_2 is decreasing with increasing distance of the original CO_2 emplacement. From that point, the dissolution rate starts to decrease (Figure 38).

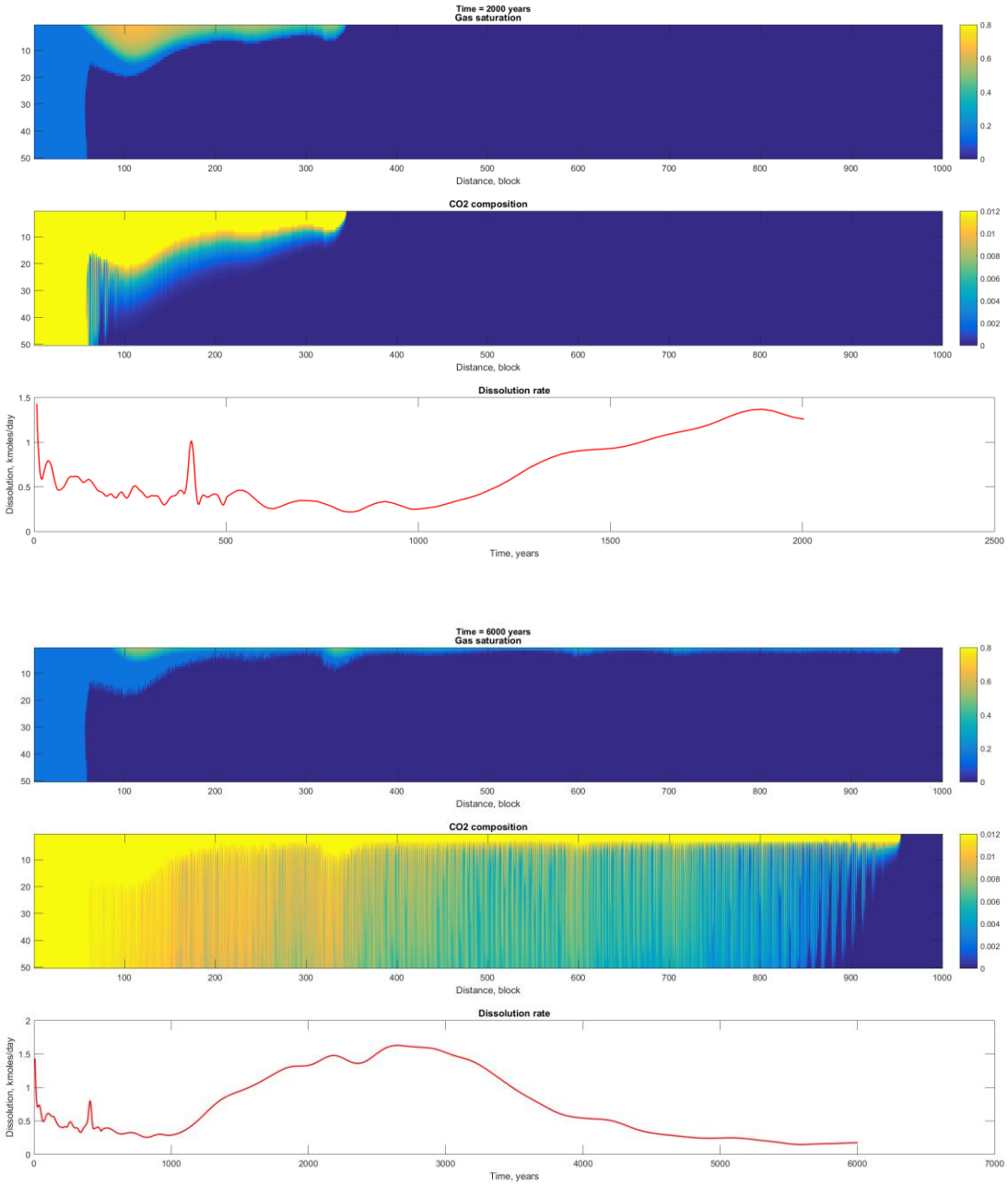

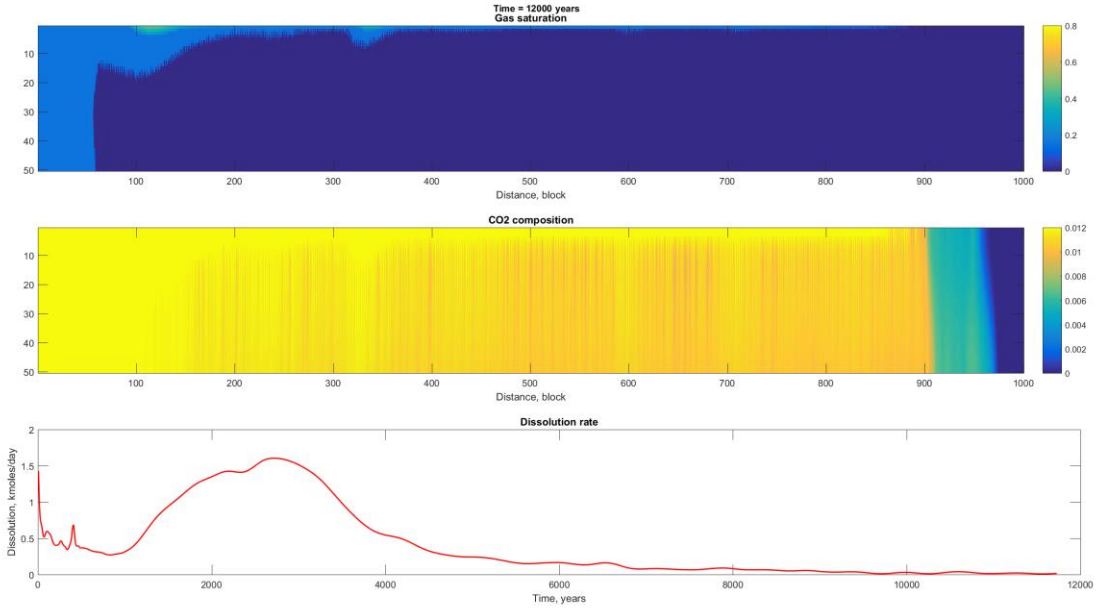

Figure 38: Gas saturation, CO_2 composition and dissolution rate into single-phase brine based on a slice from the Johansen formation for the dx20 model.

The inclinations for the Johansen formation slice calculated with equation (18) are then used to control the sink term for the proxy model. Here, the proxy model is the model without diffusion and dissolution but with a reduction by a specified rate. This specified rate for the Johansen formation was calculated in the following way: the calculated inclinations were assigned to a round inclination value (Table 9). For all these inclinations, the three important parameters were derived from the small-scale models (Table 7). The differences between the successive inclination parameter values was calculated and divided by 10. In this way, we have obtained the value in parameters between two successive parameters for every 0.1°. The outcome of the inclinations was then multiplied by the value of the parameter and added (or subtracted) to the fixed inclination parameter value. An example of the token steps to go from the three parameters obtained from small-scale (Table 7) to the parameters to implement as sink term for the Johansen formation slice are shown in Figure 39.

Table 9: inclination in Johansen formation slice assigned to inclination value with a fixed rate.

Inclination from region	Assigned to inclination
-0.5°-0.5°	0°
0.5°-1.5°	1°
1.5°-2.5°	2°
2.5°-3.5°	3°
3.5°-4.5°	4°
4.5°-5.5°	5°
5.5°-6.5°	6°
6.5°-7.5°	7°
7.5°-8.5°	8°
8.5°-9.5°	9°

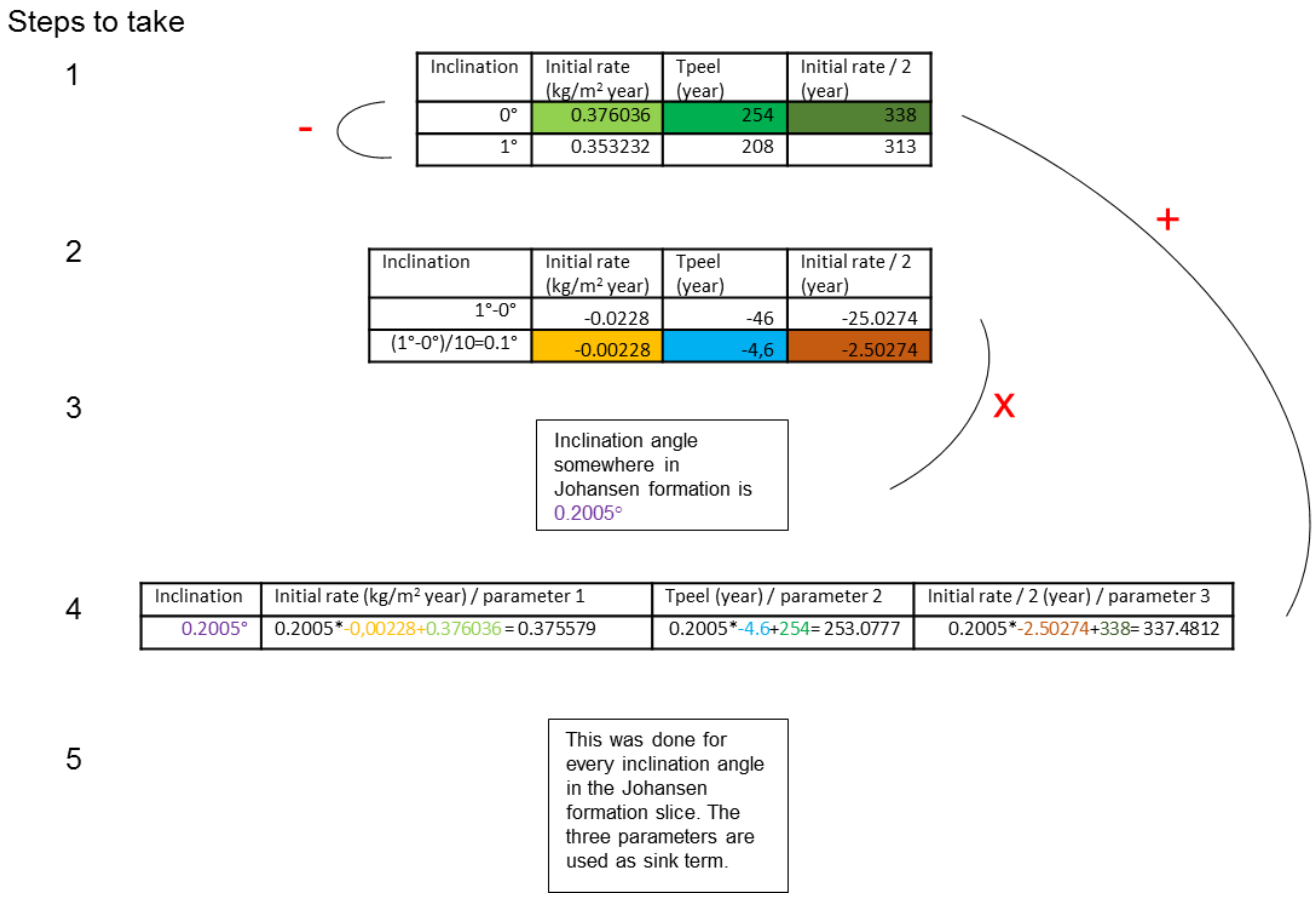

Figure 39: Steps to take to go from the three parameters obtained from small-scale, to what to implement as sink term for Johansen formation slice.

The three parameters calculated for the Johansen formation slice based on the steps as shown in Figure 39 were used as sink term for the proxy model (without diffusion and dissolution). Running this model, gave us results with which we could plot the tip position of the proxy model. The tip position was also plotted for the Johansen formation slice with dissolution and diffusion (full physics) with respect to grid resolution (dx1, dx4, dx20, dx100, and dx400) (Figure 40).

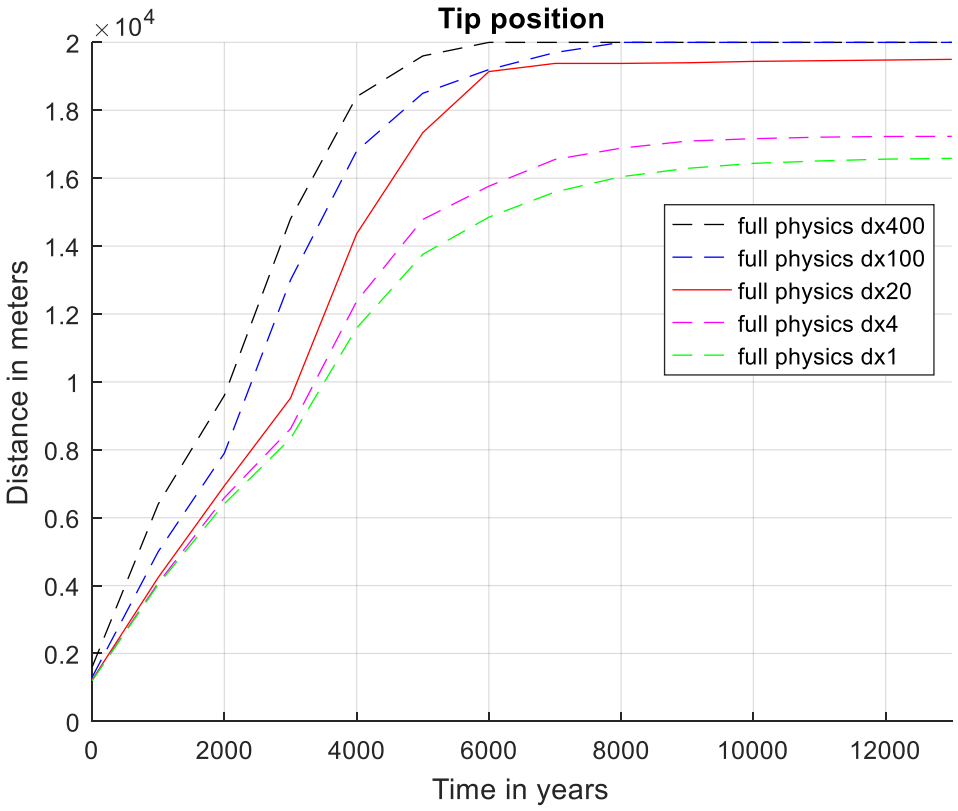

Figure 40: Tip position for the different models.

Since the grid resolution of dx20 is showing quite similar results compared to the dx4 and dx1, but it takes much less time, we implemented the rate with inclination in a reservoir with a grid block resolution of dx20. We ran a proxy model with sink term implemented in response to the inclinations in the Johansen slice (named as rate with incl dx20 in Figure 41). Another proxy model without inclination, so with a constant rate (named as rate with no-incl dx20 in Figure 41). And a final model with no dissolution (named as no dissolution dx 20 in Figure 41). Also the full physics model of dx20 and dx1 are compared in Figure 41. To show the difference between the proxy model results better, we zoomed the figure (Figure 42). The finer the model, the less far the tip position reaches. Anyhow, the rate implementation reaches a tip position in between dx20 and dx1. However, the difference between the rates implemented when considering the inclinations in the Johansen slice are not much different compared to the rate implemented with a contact rate without inclination. So full physics without rate reduction is way off comparing to the resolved case. This is because in real aquifer formations, the height differences are not so large. The used slice of the Johansen formation had an average inclination of 0.10°.

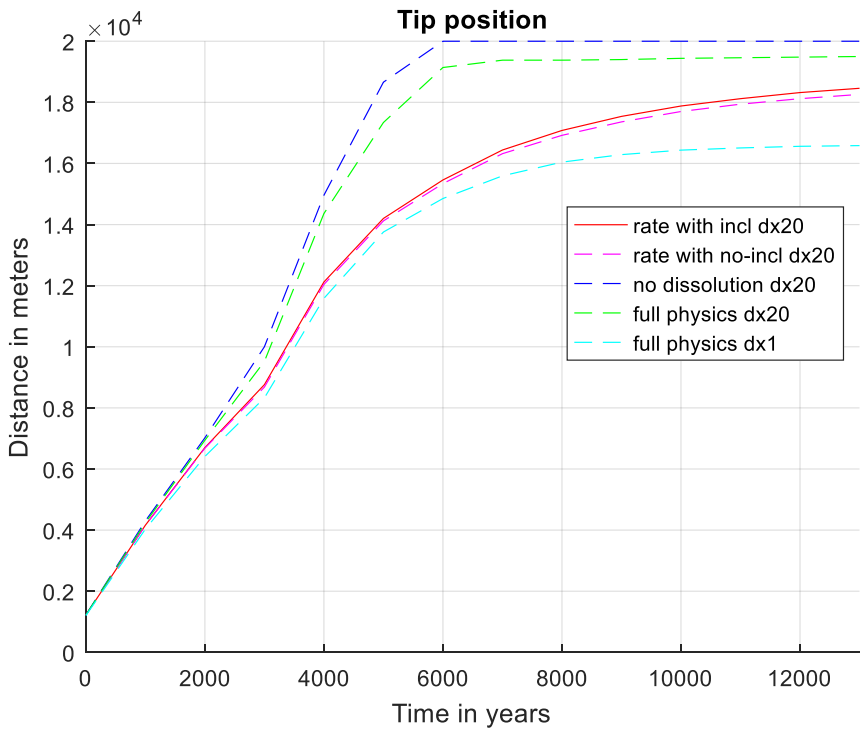

Figure 41: tip position for the proxy model: rate without inclination, rate with inclination and no dissolution rate compared to the free physic models: dx20 and dx1.

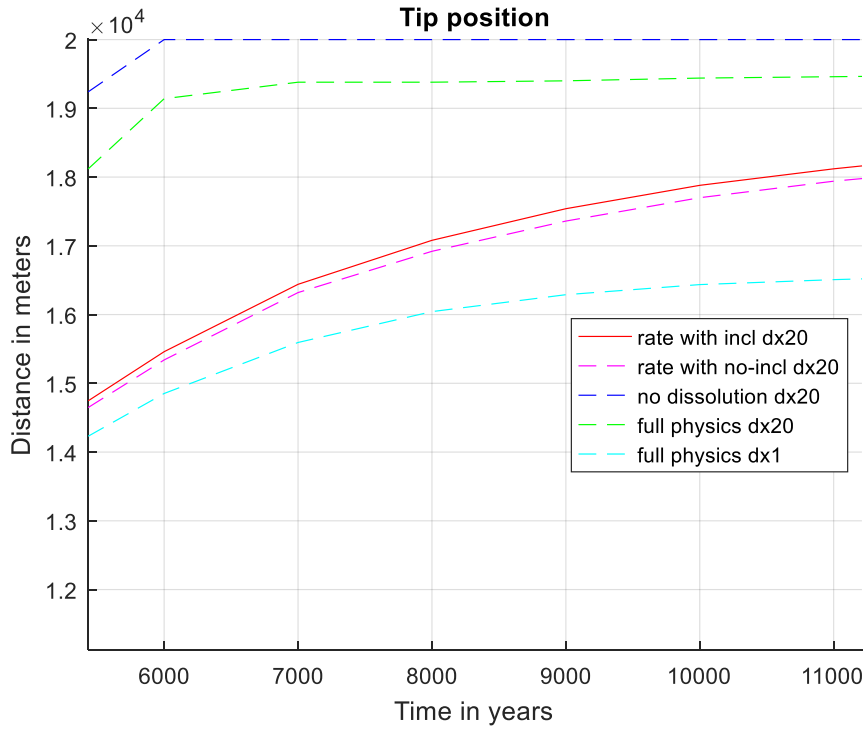

Figure 42: zoomed version of Figure 41.

Furthermore, the accuracy of the implemented rate with inclination for grid block resolution dx20 is the highest when comparing this to grid block resolutions dx100 and dx400 (Figure 43). Even though it consumes more time than the models with the resolution of dx100 and dx400 (Table 10), the time it consumes is less than the full physics model with resolution dx20, also a way less time consumption compared to resolution dx8 and dx4 (Table 8).

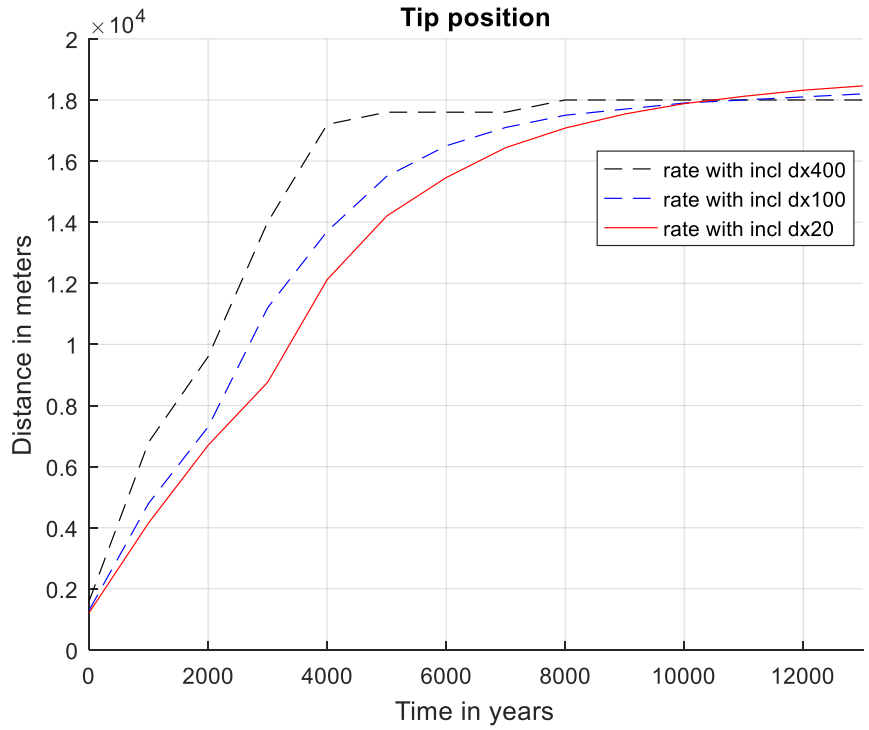

Figure 43: Tip position for the proxy model with inclination for different resolutions: dx400, dx100 and dx20.

Table 10: Running time for proxy model with inclination for different resolutions: dx400, dx100 and dx20.

Model resolution	Run time in hours
dx400	4,63
dx100	11,60
dx20	46,73

Next, we ran simulation for full physics without inclination and with 5° of inclination for the Johansen formation slice. We found that the difference in tip position is big (Figure 44).

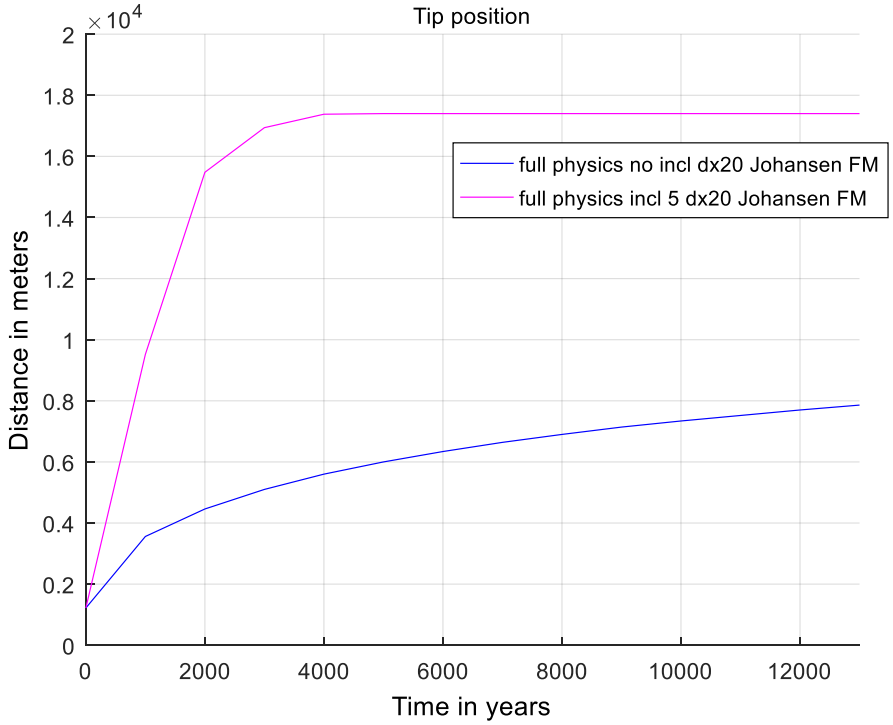

Figure 44: Tip position for full physics for grid resolution dx20, without and with 5° of inclination.

Start om Heading 1 toe te passen op de tekst die u hier wilt weergeven.

7

Conclusions

In this research, we have investigated the behaviour of CO_2 plume in a non-sloping and a sloping aquifer for small- and large-scale reservoirs. We first used small-scale models so that we later could convert to an upscaled model. Finer and coarser simulations were compared to one another. Coarser simulation (dx=1.25m and dz=1m) yielded a lower CFL averaged by time steps, but the simulation time needed was much shorter. In addition, the influence of the domain height to the small-scale simulation was studied. A simulation for a height of 25m, 50m, 75m and 100m was investigated. We have found that the smaller the height, the more the diffusion will be decreased and therefore, the dissolution rate starts to decrease. We have used a domain of 400m x 50m, that gave accurate results for plume migration and dissolution rate, but also in a proper time. A larger domain would take too much time. Compared to previous researches, we have not improved the spatial resolution and used dx=1m and dz=1m resolution for small-scale simulations. However, the results showed to be accurate enough with this resolution, a higher resolution was therefore not needed.

The slope for the small-scale model was also examined. The higher the inclination, the longer it takes until the t_{peel} is being reached. At the same time, the higher the inclination becomes, the lower the initial dissolution rate is. This is necessary to consider when using the parameters for a simplified two-phase simulation with an added sink term. The sink term acted as a surrogate for the CO_2 dissolution in the water phase. This term was therefor only applied to blocks at the interface. From the 400m x 50m domain, the parameters for the implementation of the sink term in ADGPRS could be distracted. Thus, we have performed convective mixing simulations in smaller domain to underset the results of the large-scale regarding the plume migration and trapping. Regarding the large-scale, the smaller the grid block size is the higher the dissolution rate reaches. A dx1, dx2, dx4, dx8 or dx20 does not significantly differ from one another. Since the highest dissolution rate, and the lowest in time consumption was the dx20 model, we have continued with the grid block resolution of dx20 for the case study. The case study (proxy model with implementation of sink term) showed to be more accurate than the full physics with grid block resolution of dx20, but less accurate than dx1. The proxy model with an inclined rate and a not inclined- constant rate is comparable to one another. However, the model with inclined rate is slightly better. This is since in real formations, the inclinations appeared to be less than was expected. For the cross-section of a Johansen formation, the average inclination is low, namely 0.1°. However, from the full physics we can conclude that the inclination affects the rate of CO_2 significantly. The proxy model with dissolution rate proves to be less scale dependent than the full physics models. Applying the rate improves the performance of simulation. We can conclude that the implementation of the rate with inclination takes less time than the full physics dx20, dx8 and dx4, while the accuracy is comparable to the models with resolutions between dx1-dx20. With this we found a way of reducing the time, and getting a better dissolution rate prediction. This technology seems promising, but it still needs more research. Thus, the multi-scale approach for numerical modelling of subsurface CO_2 sequestration process can be applied for practical investigations.

om Heading 1 toe te passen op de tekst die u hier wilt weergeven.

8

Future work

Since we found a way of reducing the time, and getting a better dissolution rate prediction. This technology seems promising, but it still needs more research. Therefore we better do different inclinations with the very high resolution of dx1. We expected that the Johansen formation slice would have much larger differences, but then we realized that it is better to use also high resolution inclinations, but the moment we realized, this would be too time consuming. The highest resolution takes 2,5 months. But this is definitely something for future work. The results would be closer to the resolved case. Also obtaining and plotting the storage capacity is future work for the different cases.

:art om Heading 1 toe te passen op de tekst die u hier wilt weergeven.

9

References

Ashcroft, S. J., & Isa, M. B. (1997). Effect of Dissolved Gases on the Densities of Hydrocarbons. *Journal of Chemical & Engineering Data, 42*(6), 1244-1248. doi:10.1021/je9701588

Bachu, S., Gunter, W. D., & Perkins, E. H. (1994). Aquifer disposal of CO2: Hydrodynamic and mineral trapping. *Energy Conversion and Management, 35*(4), 269-279. doi:http://dx.doi.org/10.1016/0196-8904(94)90060-4

Bai, Y., Wang, J., Fang, D., Zhang, D., & Song, J. (2014). Mechanics for the World: Proceedings of the 23rd International Congress of Theoretical and Applied Mechanics, ICTAM2012Mechanisms for Geological Carbon Sequestration. *Procedia IUTAM, 10*, 319-327. doi:http://dx.doi.org/10.1016/j.piutam.2014.01.027

Bickle, M., Chadwick, A., Huppert, H. E., Hallworth, M., & Lyle, S. (2007). Modelling carbon dioxide accumulation at Sleipner: Implications for underground carbon storage. *Earth and Planetary Science Letters, 255*(1), 164-176.

Class, H., Ebigbo, A., Helmig, R., Dahle, H. K., Nordbotten, J. M., Celia, M. A., . . . Wei, L. (2009). A benchmark study on problems related to CO2 storage in geologic formations. *Computational Geosciences, 13*(4), 409. doi:10.1007/s10596-009-9146-x

Dahle, H. K., Eigestad, G. T., Nordbotten, J. M., & Pruess, K. (2009). *A model-oriented benchmark problem for CO2 storage.* Paper presented at the Workshop on Modeling and Risk of Assessment of Geological Storage of CO2.

Elenius, M., Tchelep, H. A., & Johannsen, K. (2010). Co2 trapping in sloping aquafiers: High resolution numerical simulations. *Convective mixing in geological carbon storage*.

Elenius, M. T., Nordbotten, J. M., & Kalisch, H. (2014). Convective mixing influenced by the capillary transition zone. *Computational Geosciences, 18*(3), 417-431. doi:10.1007/s10596-014-9415-1

Elenius, M. T., Voskov, D. V., & Tchelepi, H. A. (2015). Interactions between gravity currents and convective dissolution. *Advances in Water Resources, 83*, 77-88. doi:http://dx.doi.org/10.1016/j.advwatres.2015.05.006

Eigestad, G. T., Dahle, H. K., Hellevang, B., Riis, F., Johansen, W. T., & Øian, E. (2009). Geological modeling and simulation of CO 2 injection in the Johansen formation. *Computational Geosciences*, *13*(4), 435-450.

Farajzadeh, R., Salimi, H., Zitha, P. L. J., & Bruining, H. (2007). Numerical simulation of density-driven natural convection in porous media with application for CO2 injection projects. *International Journal of Heat and Mass Transfer, 50*(25–26), 5054-5064. doi:http://dx.doi.org/10.1016/j.ijheatmasstransfer.2007.08.019

Farajzadeh, R., Zitha, P. L. J., & Bruining, J. (2009). Enhanced Mass Transfer of CO2 into Water: Experiment and Modeling. *Industrial & Engineering Chemistry Research, 48*(13), 6423-6431. doi:10.1021/ie801521u

Garipov, T.T., Karimi-Fard, M., Tchelepi, H.A.: Discrete fracture model for coupled flow and geomechanics (2016) Computational Geosciences, 20 (1), pp. 149-160.

Gasda, S. E., Nordbotten, J. M., & Celia, M. A. (2009). Vertical equilibrium with sub-scale analytical methods for geological CO_2 sequestration. *Computational Geosciences*, *13*(4), 469-481.

Gasda, S., Nordbotten, J., & Celia, M. (2011). Vertically averaged approaches for CO2 migration with solubility trapping. *Water Resources Research, 47*(5).

Gasda, S. E., Nordbotten, J. M., & Celia, M. A. (2012). Application of simplified models to CO 2 migration and immobilization in large-scale geological systems. *International Journal of Greenhouse Gas Control, 9*, 72-84.

Hangx, S. (2005). Subsurface mineralisation. Rate of CO2 mineralisation and geomechanical effects on host and seal formations. Behaviour of the CO2-H2O system and preliminary mineralisation model and experiments.

Hassanzadeh, H., Pooladi-Darvish, M., & Keith, D. (2005). Modelling of Convective Mixing in CO Storage. *Journal of Canadian Petroleum Technology, 44*(10).

Hesse, M. A. (2008). *MATHEMATICAL MODELING AND MULTISCALE SIMULATION OF C02 STORAGE IN SALINE AQUIFERS* (Doctoral dissertation, Stanford University).

Johnson, J., Nitao, J., Steefel, C., & Knauss, K. (2001). *Reactive transport modeling of geologic CO 2 sequestration in saline aquifers.* Paper presented at the The Influence of Intra-Aquifer Shales and the Relative Effectiveness of Structural, Solubility, and Mineral Trapping During Prograde and Retrograde Sequestration. Washington: First National Conference on Carbon Sequestration.

Kemmere, M. F., & Meyer, T. (2006). *Supercritical carbon dioxide: in polymer reaction engineering*: John Wiley & Sons.

King, M., MacDonald, D., Todd, S., & Leung, H. (1998). *Application of novel upscaling approaches to the Magnus and Andrew reservoirs.* Paper presented at the European Petroleum Conference.

King, M., & Mansfield, M. (1999). Flow simulation of geologic models. *SPE Reservoir Evaluation & Engineering, 2*(04), 351-367.

McBride-Wright, M., Maitland, G. C., & Trusler, J. M. (2014). Viscosity and Density of Aqueous Solutions of Carbon Dioxide at Temperatures from (274 to 449) K and at Pressures up to 100 MPa. *Journal of Chemical & Engineering Data, 60*(1), 171-180.

McPherson, B. J. O. L., & Cole, B. S. (2000). Multiphase CO2 flow, transport and sequestration in the Powder River Basin, Wyoming, USA. *Journal of Geochemical Exploration, 69–70*, 65-69. doi:http://dx.doi.org/10.1016/S0375-6742(00)00046-7

Metz, B., Davidson, O., De Coninck, H., Loos, M., & Meyer, L. (2005). IPCC, 2005: IPCC special report on carbon dioxide capture and storage. Prepared by Working Group III of the Intergovernmental Panel on Climate Change. *Cambridge, United Kingdom and New York, NY, USA, 442*.

Metz, B., Davidson, O., De Coninck, H., Loos, M., & Meyer, L. (2005a). Carbon dioxide capture and storage.

Metz, B., Davidson, O., De Coninck, H., Loos, M., & Meyer, L. (2005b). IPCC, 2005: IPCC special report on carbon dioxide capture and storage. Prepared by Working Group III of the Intergovernmental Panel on Climate Change. *Cambridge, United Kingdom and New York, NY, USA, 442*.

Mo, S., Zweigel, P., Lindeberg, E. G., & Akervoll, I. (2005). *Effect of geologic parameters on CO2 storage in deep saline aquifers.* Paper presented at the SPE Europec/EAGE Annual Conference.

Nordbotten, J. M., & Dahle, H. K. (2011). Impact of the capillary fringe in vertically integrated models for CO2 storage. *Water Resources Research, 47*(2).

Pruess, K., & Müller, N. (2009). Formation dry-out from CO2 injection into saline aquifers: 1. Effects of solids precipitation and their mitigation. *Water Resources Research, 45*(3).

Pruess, K., & Nordbotten, J. (2011). Numerical Simulation Studies of the Long-term Evolution of a CO2 Plume in a Saline Aquifer with a Sloping Caprock. *Transport in Porous Media, 90*(1), 135-151. doi:10.1007/s11242-011-9729-6

Riaz, A., Hesse, M., Tchelepi, H., & Orr, F. (2006). Onset of convection in a gravitationally unstable diffusive boundary layer in porous media. *Journal of Fluid Mechanics, 548*(1), 87-111.

Rubin, E. S. (2006). Summary of the IPCC special report on carbon dioxide capture and storage.

Shamshiri, H., & Jafarpour, B. (2012). Controlled CO2 injection into heterogeneous geologic formations for improved solubility and residual trapping. *Water Resources Research, 48*(2). .

Szulczewski, M., Hesse, M., & Juanes, R. (2013). Carbon dioxide dissolution in structural and stratigraphic traps. *Journal of Fluid Mechanics, 736*, 287-315.

Xu, X., Chen, S., & Zhang, D. (2006). Convective stability analysis of the long-term storage of carbon dioxide in deep saline aquifers. *Advances in Water Resources, 29*(3), 397-407.

Zaydullin, R., Voskov, D., James, S., Lucia, A.: Fully compositional and thermal reservoir simulation. Computers and Chemical Engineering 63, 51 – 65 (2014)

Zhang, Y., Chang, F., Song, Y., Zhao, J., Zhan, Y., & Jian, W. (2011). Density of Carbon Dioxide + Brine Solution from Tianjin Reservoir under Sequestration Conditions. *Journal of Chemical & Engineering Data, 56*(3), 565-573. doi:10.1021/je101214e